Boundary-Layer Meteorol
DOI 10.1007/s10546-009-9404-4

ARTICLE

Exploring the Effects of Microscale Structural Heterogeneity of Forest Canopies Using Large-Eddy Simulations

Gil Bohrer · Gabriel G. Katul · Robert L. Walko · Roni Avissar

Received: 29 July 2008 / Accepted: 15 June 2009

Abstract The Regional Atmospheric Modeling System (RAMS)-based Forest Large-Eddy Simulation (RAFLES), developed and evaluated here, is used to explore the effects of three-dimensional canopy heterogeneity, at the individual tree scale, on the statistical properties of turbulence most pertinent to mass and momentum transfer. In RAFLES, the canopy interacts with air by exerting a drag force, by restricting the open volume and apertures available for flow (i.e. finite porosity), and by acting as a heterogeneous source of heat and moisture. The first and second statistical moments of the velocity and flux profiles computed by RAFLES are compared with turbulent velocity and scalar flux measurements collected during spring and winter days. The observations were made at a meteorological tower situated within a southern hardwood canopy at the Duke Forest site, near Durham, North Carolina, U.S.A. Each of the days analyzed is characterized by distinct regimes of atmospheric stability and canopy foliage distribution conditions. RAFLES results agreed with the 30-min averaged flow statistics profiles measured at this single tower. Following this intercomparison, two case studies are numerically considered representing end-members of foliage and midday atmospheric stability conditions: one representing the winter season with strong winds above a sparse canopy and a slightly unstable boundary layer; the other representing the spring season with a dense canopy, calm conditions, and a strongly convective boundary layer. In each case, results from the control canopy, simulating the observed heterogeneous canopy structure at the Duke Forest hardwood stand, are compared with a test case that also includes heterogeneity commensurate in scale to tree-fall gaps. The effects of such tree-scale canopy heterogeneity on the flow are explored at three levels pertinent to

G. Bohrer · G. G. Katul · R. L. Walko · R. Avissar
Department of Civil and Environmental Engineering, Duke University, Durham, NC 27708, USA

G. Bohrer (✉)
Department of Civil and Environmental Engineering and Geodetic Science, Ohio State University,
470 Hitchcock Hall, 2070 Neil Ave., Columbus, OH 43210, USA
e-mail: bohrer.17@osu.edu

G. G. Katul
Nicholas School of the Environment, Duke University, Durham, NC 27708, USA

Published online: 30 June 2009

biosphere-atmosphere exchange. The first level (zero-dimensional) considers the effects of such heterogeneity on the common representation of the canopy via length scales such as the zero-plane displacement, the aerodynamic roughness length, the surface-layer depth, and the eddy-penetration depth. The second level (one-dimensional) considers the normalized horizontally-averaged profiles of the first and second moments of the flow to assess how tree-scale heterogeneities disturb the entire planar-averaged profiles from their canonical (and well-studied planar-homogeneous) values inside the canopy and in the surface layer. The third level (three-dimensional) considers the effects of such tree-scale heterogeneities on the spatial variability of the ejection-sweep cycle and its propagation to momentum and mass fluxes. From these comparisons, it is shown that such microscale heterogeneity leads to increased spatial correlations between attributes of the ejection-sweep cycle and measures of canopy heterogeneity, resulting in correlated spatial heterogeneity in fluxes. This heterogeneity persisted up to four times the mean height of the canopy (h_c) for some variables. Interestingly, this estimate is in agreement with the working definition of the thickness of the canopy roughness sublayer ($2h_c$–$5h_c$).

Keywords Atmospheric modelling · Atmospheric boundary layer · Backscatter · Biosphere–atmosphere interactions · Land-surface heterogeneity · Large-eddy simulation · Tree canopy · Turbulence · Regional Atmospheric Modeling System

1 Introduction

Atmospheric turbulence controls the exchange of moisture, CO_2 and other gases from plant canopies into the atmosphere, and also affects the onset, propagation and termination of a diverse array of biological transport phenomena, such as seed dispersal, pathogen spread, and the dispersion of volatile organic compounds. Not surprisingly, the interplay between land-surface heterogeneity and turbulent mass and energy transport has received significant attention across a wide range of heterogeneity scales varying from the macroscale (created by differences between geographic regions), the mesoscale (as a result of differences between land cover types), and more recently the microscale, at which canopy variability is the result of a mosaic of forested and grassy patches [O(200 m)] (e.g., Collins and Avissar 1994; Li and Avissar 1994; Dias and Regnier 1996; Fisch et al. 1996; Liu and Avissar 1996; Scanlon and Albertson 2003; Bou-Zeid et al. 2007; Juang et al. 2007; Cassiani et al. 2008; Detto et al. 2008; Dupont and Brunet 2008b).

However, heterogeneity at an even finer scale, viz. the scale of tree crowns and tree-fall gaps [O(5–50 m)], has rarely been considered despite its potential impact on these exchanges as well as the dislodging of inertial particles such as seeds and pollen in forested ecosystems. It has been recently demonstrated that such small-scale heterogeneity effects may change the far tail of the dispersion probability density function of seed and pollen (Bohrer et al. 2008b). Moreover, these finer scales may pose challenges to the interpretation of tower-based eddy-covariance flux measurements, though their effects have rarely been considered in the long-term monitoring of scalar fluxes (Baldocchi et al. 2000), except at a few sites (Katul et al. 1999; Oren et al. 2006). Footprint methods that are commonly used to relate point observations on towers to sources that are contributing to these tower-measured fluxes (Raupach 1989a,b; Hsieh et al. 2000, 2003; Rannik et al. 2000; Schäfer 2002) still encounter challenges over heterogeneous canopies though the effects of some types of heterogeneity are receiving increased attention (Finnigan 2004; Foken and Leclerc 2004; Kruijt et al. 2004; Sogachev et al. 2005; Detto et al. 2006; Belcher et al. 2008).

There are good reasons why the impacts of these fine-scale heterogeneities on turbulent fluxes have not been historically explored. Turbulent mixing within the atmosphere is often thought to be sufficiently effective in 'averaging-out' the influence of fine-scale variability (i.e. at scales where the heterogeneity length scale is much smaller than the largest flux-transporting eddies). However, inside forested canopies, flux-transporting eddies occur at a scale comparable to the crown size (Raupach et al. 1996; Katul et al. 1998; Katul and Chang 1999; Massman and Weil 1999; Finnigan 2000; Poggi et al. 2004c; Launiainen et al. 2007). Experimental investigations in the field are logistically difficult to carry out given the high resolution and the three-dimensional nature of the required data, but computational simulation methods, especially Large-Eddy Simulations (LES), and computational infrastructure have now progressed enough to permit preliminary assessments of these effects, the subject of this study.

In recent years, a number of LES reported on some of the effects of canopy heterogeneity on the flow statistics, representing these effects through the bottom boundary condition to the flow (Bou-Zeid et al. 2004, 2007; Stoll and Porte-Agel 2006b). Some LES studies have resolved the mean vertical structure of the leaf area density profile in a horizontally homogeneous canopy (e.g., Shaw et al. 1988; Su et al. 1998; Shaw and Patton 2003), and more recently, LES studies have combined vertical structure with horizontal heterogeneity (e.g., Albertson et al. 2001; Kanda et al. 2004; Yang et al. 2006a,b; Cassiani et al. 2008; Dupont and Brunet 2008b). The main outcome is that the vertical canopy structure and 'large horizontal gaps' do indeed modify turbulence from its planar-homogeneous form inside and above the canopy layer. Yue et al. (2007, 2008) have shown that plant-scale grid resolution improves the flow simulation within the canopy, perhaps indicating that finer scale heterogeneity plays a significant role. However, within the context of these sub-tree-scale effects, the existing formulations within current LES use several assumptions that may not be advantageous when exploring such fine-scale heterogeneities. For example, the assumption of horizontal, patch-level homogeneity, i.e., horizontal heterogeneity, exists only between patch types at a scale much coarser than the diameter of individual tree crowns and the height of the canopy. Existing formulations only deal with a horizontally constant, mean vertical profile of leaf area density within a patch type. Moreover, many canopy LES have a restricted vertical domain and do not include a dynamic representation of the full boundary-layer eddies. Finally, existing canopy LES models assume that the vegetation mainly exerts drag on the flow but do not account for the canopy's effective volume (i.e., the canopy has infinite porosity). Hence, to make progress on the issues of fine-scale heterogeneity, the existing LES formulations must be revised.

The Regional Atmospheric Modeling System (RAMS)-based Forest LES (hereafter referred to as "RAFLES"), which is presented herein, explicitly resolves turbulence in realistic, observation-based, three-dimensional (3-D) heterogeneous canopies. RAFLES' parent model, RAMS (Pielke et al. 1992), is a regional atmospheric model with grid nesting capabilities that operate as LES (e.g., Avissar et al. 1998; Avissar and Schmidt 1998), and solves the Navier–Stokes (N–S) equations, using a quasi-hydrostatic approach and the Boussinesq approximation, on a rectangular, vertically stretched grid mesh.

RAFLES includes a multi-layer, 3-D heterogeneous canopy, allowing for the effects of leaves and stems on the drag and fluxes and also for the physical barrier created by the stems and branches. Its typical grid-cell volume, of the order of $1 \times 1 \times 1\,\mathrm{m}^3$ ($5 \times 5 \times 3\,\mathrm{m}^3$ was used here) allows for the simulation of many of the turbulence features that are generated by tree-crown structures. Its simulation domain, typically on the order of $1 \times 1 \times 1\,\mathrm{km}^3$ (here, $1.28 \times 1.28 \times 1.41\,\mathrm{km}^3$) is large enough to simulate a fully dynamic boundary layer with its rich eddy-size structure.

We describe RAFLES and evaluate its performance against field observations; the model is then used to explore the effects of tree-scale canopy heterogeneity (corresponding to the micro-γ scale as defined by Orlanski 1975) on the spatial dynamics of ejection and sweep events for two end-members of atmospheric stability and foliage states.

2 Model Description

2.1 Notation

All variables are decomposed into two components, $\varphi = \overline{\varphi} + \varphi'$, where $\overline{\varphi}$ is the resolved, grid-averaged component, and φ' is the perturbation from that mean [i.e., the subgrid-scale (SGS) perturbation] defined such that $\overline{\varphi'} = 0$. For numerical purposes, some variables are decomposed into a horizontally homogeneous, temporally-averaged reference state, marked by a subscript "0", and a heterogeneous, temporally variable perturbation, marked by a subscript "p", i.e., $\varphi = \varphi_0 + \varphi_p$. Angled brackets, $\langle\,\rangle$, mark a domain-wise horizontal averaging and has been used for analyzing the model output and for forcing of the horizontal wind. A tilde indicates a typical averaging period (also used for data analysis), chosen here to be 30 min for consistency with the common eddy-covariance tower-based averaging periods.

2.2 Governing Equations

RAFLES solves the set of compressible, N–S equations written in quasi-Boussinesq form, and where pressure is expressed in terms of the Exner function, π:

$$\pi = c_p \left(\frac{p}{p_{00}}\right)^{\frac{R_d}{c_p}} = \frac{c_p T}{\theta} = \frac{c_p T_v}{\theta_v}, \tag{1}$$

where c_p is the specific heat capacity of the air, R_d is the gas constant, p is pressure, $p_{00} = 10^5$ Pa is close to standard sea-level pressure, θ is potential temperature, θ_v is potential virtual temperature, T is air temperature, and T_v is virtual temperature. The model reference state is hydrostatically balanced according to $\partial\pi_0/\partial z = -g/\theta_{v0}$.

Applying the above-described partitioning between resolved and SGS components to the N–S equations leads to the following prognostic equation for resolved-scale velocity:

$$\begin{aligned}\frac{\partial \overline{u_i}}{\partial t} + \frac{1}{\rho_0}\left[-\overline{u_i}\frac{\partial(\rho_0 \overline{u_j})}{\partial x_j} + \frac{\partial(\rho_0 \overline{u_i u_j})}{\partial x_j} + \frac{\partial(\rho_0 \overline{u_i' u_j'})}{\partial x_j}\right] \\ = +\delta_{i3} g \frac{\overline{\theta_{vp}}}{\theta_{v0}} - 2\varepsilon_{ijk}\Omega_j\left(\overline{u_k} - \langle u_{gk}\rangle\right) - \theta_0\left(\frac{\partial \overline{\pi_p}}{\partial x_i}\right) + F(\overline{u_i}) + D_i(\overline{V}),\end{aligned} \tag{2}$$

where u_i is wind velocity, ρ is air density, t is time, g is acceleration due to gravity, δ is the Kronecker delta, u_{gk} is the geostrophic wind, the geostrophic pressure gradient is excluded from π_p, and Ω is the angular velocity of the earth. The Einstein notation is used throughout.

The left-hand side of this equation is written as a sum of flux terms by substituting the advective term $\rho_0 \overline{u_j}(\partial \overline{u_i}/\partial x_j)$ by its chain-rule equivalent $\partial\left(\rho_0 \overline{u_i u_j}\right)/\partial x_j - \overline{u_i}\left(\partial \overline{\rho_0 u_j}\right)/\partial x_j$, and expanding by the reference state density to obtain the momentum flux terms. The model neglects the vertical components of the Coriolis force (we should note that many canopy LES neglect the entire Coriolis term). Dissipation is parameterized with the SGS terms. $D_i(\overline{V})$ represents the components of the canopy drag force per unit mass that are a function of the

resolved-scale velocity (described later). In this formulation, the forcing by the geostrophic wind is transformed from the pressure gradient term (which is initialized in a horizontally homogeneous manner) to the Coriolis term. $F(\overline{u_i})$ represents the sum per unit mass of horizontal wind forcing through the domain, which is comprised of Rayleigh friction and of a Newtonian nudging term that maintains a mean mesoscale horizontal wind

$$-F(\overline{u_i}) = (1-\delta_{i3})\frac{l_{\varepsilon f}}{t_{\varepsilon f}}(\langle\overline{u_i}\rangle - \langle u_{Ii}\rangle) + \frac{l_{\varepsilon r}}{t_{\varepsilon r}}(\overline{u_i} - (1-\delta_{i3})\langle u_{gi}\rangle), \tag{3}$$

where u_{Ii} is the component of the forced mean horizontal wind profile, which is horizontally homogeneous and is also used as an initial condition, $t_{\varepsilon f}$ and $t_{\varepsilon r}$ are the dissipation time scales for horizontal velocity and gravity waves, respectively, and $l_{\varepsilon f}$ and $l_{\varepsilon r}$ are nudging coefficients for horizontal wind forcing by Newtonian nudging and for Rayleigh friction (respectively). The coefficients $l_{\varepsilon f}$ and $l_{\varepsilon r}$ are horizontally homogeneous but vary vertically throughout the domain; $l_{\varepsilon r} = 0$ everywhere except in the five uppermost layers of the domain, where it decays linearly from one in the topmost layer to zero in the fifth layer from the domain top. Also, $l_{\varepsilon f} = 1$ at elevations above four times the mean canopy-top height, it decreases linearly from one to zero at heights between four times and three times the canopy height, and it is zero below that height.

Similar derivations as in Eq. 2 lead to the other conservation equations used in RAFLES; the equation for conservation of scalars, including heat and moisture, is

$$\frac{\partial\overline{\chi}}{\partial t} = \frac{1}{\rho_0}\left[\frac{\overline{\chi}\,\partial\left(\rho_0\overline{u_j}\right)}{\partial x_j} - \frac{\partial\left(\rho_0\overline{u_j\chi}\right)}{\partial x_j} - \frac{\partial\left(\rho_0\overline{u_j'\chi'}\right)}{\partial x_j}\right] + S_\chi, \tag{4}$$

where χ is a scalar concentration, and S_χ are the sum of sources and sinks of the scalar.

The prognostic equation for the Exner function is derived from the continuity of energy (Klemp and Wilhelmson 1978):

$$\frac{\partial\overline{\pi}}{\partial t} = \frac{-c_{sp}^2}{\rho_0\theta_0^2}\frac{\partial\left(\rho_0\theta_0\overline{u_j}\right)}{\partial x_j}, \tag{5}$$

where c_{sp} is the effective speed of sound, defined below in Eq. 10.

2.3 Subgrid-Scale Parameterization of Turbulence

The prognostic equation for the SGS (filtered) turbulent kinetic energy (TKE), $\overline{e} = \overline{u_i'u_i'}/2$, is derived from the N–S equations by splitting all variables into resolved and SGS components (Deardorff 1980):

$$\frac{\partial\overline{e}}{\partial t} + \frac{\partial\left(\rho_0\overline{u_j e}\right)}{\rho_0\partial x_j} - \frac{\overline{e}}{\rho_0}\frac{\partial\left(\rho_0\overline{u_j}\right)}{\partial x_j} = \frac{g}{\overline{\theta_v}}\overline{w'\theta_v'} - \overline{u_i'u_j'}\frac{\partial\overline{u_i}}{\partial x_j} - \frac{\partial}{\partial x_i}\left(\overline{u_i'\left(e + \frac{p'}{\overline{\rho}}\right)}\right) - \frac{8}{3}C_{dl}A_l\left|\overline{V}\right|\overline{e} - \varepsilon, \tag{6}$$

where ε is the TKE dissipation rate, $e = \left(u_i - \widetilde{\langle u_i\rangle}\right)^2/2$ is the total SGS TKE, and the fourth term on the right-hand side represents the contribution of the canopy to the drag on SGS motion (Shaw and Patton 2003). We chose to neglect wake generation because this term is dependent on the effective size of wake generating elements, which is hard to define in a

forest with complex foliage distribution structure, and was found to have only a small effect on the total TKE given the size of leaves (Shaw and Patton 2003).

To evaluate the SGS-covariance terms, RAFLES adopts the Deardorff (1980) SGS parameterization (implemented in RAMS by Hadfield et al. 1991) with a backscatter term (Bhushan and Warsi 2005), which converts TKE to resolved momentum and improved turbulence scaling at higher resolutions close to the grid-mesh size. The turbulent stress can be approximated by

$$\overline{u_i' u_j'} = -K_m \left(\frac{\partial \overline{u_i}}{\partial x_j} + \frac{\partial \overline{u_j}}{\partial x_i} \right) + \frac{2}{3} \delta_{ij} \overline{e} + \alpha_1 l_g^2 \left(\frac{\partial \overline{u_i}}{\partial x_k} \frac{\partial \overline{u_j}}{\partial x_k} \right) - \alpha_2 l_g^2 \left(\frac{\partial \overline{u_k}}{\partial x_i} \frac{\partial \overline{u_k}}{\partial x_j} \right), \quad (7)$$

where $l_g = (1.5^2 \Delta x \Delta y \Delta z)^{1/3}$ is an empirical length scale that characterizes the mesh size (Patton 1997), Δx, Δy, and Δz are the grid spacings, and $\alpha_1 = 1/12$ and $\alpha_2 = 0.0336$ are the backscatter coefficients (Bhushan and Warsi 2005; Bhushan et al. 2006). K_m and K_h are the turbulence diffusivity for momentum and scalars (respectively), and along with the other terms in Eq. 6, they are evaluated according to Deardorff (1980). The transport of TKE can be approximated by

$$\overline{u_i' \left(e + \frac{p'}{\overline{\rho}} \right)} = -2 K_m \frac{\partial \overline{e}}{\partial x_i}, \quad (8)$$

the scalar flux (including water vapour) is approximated by

$$\overline{u_i' \chi'} = -K_h \left(\frac{\partial \overline{\chi}}{\partial x_i} \right), \quad (9)$$

and the vertical flux of virtual temperature is approximated by

$$\overline{w' \theta_v'} = -K_h \left(A \frac{\partial \overline{\theta_l}}{\partial z} + B \overline{\theta} \frac{\partial \overline{q}}{\partial z} \right), \quad (10)$$

where q is specific humidity, and A and B are empirical functions defined as follows:

$$A = \begin{cases} 1 + 0.61 \overline{q} & \text{Unsaturated air} \\ 1 + 0.61 \overline{q} - A_q & \text{Saturated air} \end{cases} \quad (11a)$$

$$B = \begin{cases} 0.61 & \text{Unsaturated air} \\ \frac{c_v}{c_p \overline{T}} - 1 & \text{Saturated air} \end{cases} \quad (11b)$$

where A_q is a correction for saturated air expressed as:

$$A_q = 0.622 \left(\frac{c_v \overline{q_s}}{R_d \overline{T}} \right) \left(\frac{c_v (1 + 0.61 \overline{q})}{c_p \overline{T}} - 1.61 \right) \left(1 + \frac{0.622 c_v^2 \overline{q_s}}{R_d c_p \overline{T}^2} \right)^{-1}. \quad (12)$$

Here q_s is the specific saturation humidity, c_v is the latent heat of vaporization, and K_m and K_h are defined as:

$$K_m = 0.1 l_\varepsilon \overline{e}^{1/2}, \quad (13a)$$

$$K_h = K_m \left(1 + 2 \frac{l_\varepsilon}{l_g} \right), \quad (13b)$$

where l_ε is an empirical length scale for mesh size and dissipation, defined in a convective boundary layer as:

$$l_\varepsilon = \min\left(l_g, 0.76\bar{e}^{1/2}\left(\frac{g}{\overline{\theta_v}}\frac{\partial\overline{\theta}}{\partial z}\right)^{-1/2}\right). \tag{14}$$

The dissipation rate is approximated by

$$\varepsilon = \frac{\left(0.19 + \frac{0.51 l_\varepsilon}{l_g}\right)\bar{e}^{\frac{3}{2}}}{3l_\varepsilon}. \tag{15}$$

2.4 Numerical Scheme

Equations 3–7 form a closed set and can be discretized in time and space and solved numerically; RAFLES uses a shaved grid-cell finite volume discretization (Adcroft et al. 1997; Walko and Avissar 2008). Generally, to convert any flux term with a derivative in the i direction, the term is multiplied by the aperture area in the plane normal to the derivative, $\sigma_i = \Delta x_j \Delta x_k$, where $i \neq j; i \neq k; j < k$, ($j, k$ define the plane normal to i and are counted only once). Control volume integrals of divergence quantities are transformed to surface integrals through the application of the Gauss divergence theorem,

$$\int_\Psi \nabla\cdot\vec{\Phi}d\Psi = \oint_\sigma \vec{\Phi}\cdot d\vec{\sigma} \equiv \sum_{i=1}^{3}\frac{\dot{\Delta}_i(\sigma_i\Phi_i)}{\Psi}, \tag{16}$$

where $\vec{\Phi}$ represents any vector variable in the grid cell, $\oint$ indicates a volume integral over the grid cell, $\Psi = \Delta x_1 \Delta x_2 \Delta x_3$ is the grid-cell volume, and $\dot{\Delta}_i()$ represents the difference between values on parallel faces of a grid parcel.

RAFLES uses a split-time leapfrog discretization scheme (Haltiner and Williams 1980). After substituting the eddy-covariance terms back into the velocity equation (Eq. 2), this equation is discretized in space and time as follows:

$$\begin{aligned}
&\frac{\overline{u_i}^{(t+1)} - \overline{u_i}^{(t-1)}}{2\Delta t} \\
&\quad + \frac{M}{N_{ts}}\sum_{m=1}^{N_{ts}/M}\left[\frac{\dot{\Delta}_j}{\rho_0\Psi}\left(\left(\rho_0\sigma_j\overline{u_i u_j}\right) - \overline{u_i}\left(\rho_0\sigma_j\overline{u_j}\right) - \rho_0\sigma_j K_m\left(\frac{\Delta\overline{u_i}}{\Delta x_j} + \frac{\Delta\overline{u_j}}{\Delta x_i}\right)\right.\right. \\
&\quad \left.\left. + \left(\rho_0\sigma_j\frac{2}{3}\delta_{ij}\bar{e} + \rho_0\sigma_j l_g^2\left(\alpha_1\left(\frac{\Delta\overline{u_i}}{\Delta x_k}\frac{\Delta\overline{u_j}}{\Delta x_k}\right) - \alpha_2\left(\frac{\Delta\overline{u_k}}{\Delta x_i}\frac{\Delta\overline{u_k}}{\Delta x_j}\right)\right)\right)\right)^{(t-1+m\Delta t_m)}\right] \\
&= \delta_{i3} g\frac{\overline{\theta_{vp}}^{(t)}}{\theta_{v0}} - 2\varepsilon_{ijk}\Omega_j\left(\overline{u_k}^{(t)} - u_{g_k}\right) - \frac{\theta_0}{N_{ts}}\sum_{n=1}^{N_{ts}}\left[\left(\frac{\Delta(\overline{\pi_p})}{\Delta x_i}\right)^{(t-1+n\Delta t_s)} - \frac{\Delta(\pi_g)}{\Delta x_i}\right] \\
&\quad + F\left(\overline{u_i}\right)^{(t)} + D_i\left(\overline{V}\right)^{(t)},
\end{aligned} \tag{17}$$

where the superscripts "t", "$t-1$", and "$t+1$" indicate the timestep and Δt is the largest timestep interval. The time-split method allows different terms of the equation to be integrated at different timestep intervals. The pressure gradient term is integrated (using Eq. 5) over a small timestep interval, defined as $\Delta t_s = \Delta t / N_{ts}$, where $N_{ts} \geq 1$ is the number of small timesteps within each large timestep. After each small timestep, $\overline{u_i}^{(t_s)}$ is updated. This is done

for numerical stability given the speed of acoustic pressure changes. The same process, only with an intermediate timestep, Δt_m, is applied to the advection and eddy-covariance terms. Δt_m is defined such that $\Delta t_s \leq \Delta t_m \leq \Delta t$ and $\Delta t_m = M \Delta t_s$ where $M \geq 1$ is an integer. The same time and space discretization was applied to the other governing equations in the model (Eqs. 4–6).

Additional stability is achieved in RAFLES by using the Arakawa and Lamb (1977) type-C staggered grid scheme, and by slowing the effective speed of sound in the model, c_{sp}, which is used for updating the pressure perturbations (Eq. 5), to

$$c_{sp} = c_s \min\left(1, \frac{0.95 \Delta x N_{ts}}{4 c_s \Delta t}\right), \tag{18}$$

where c_s is the physical speed of sound. In the cases simulated here, c_{sp} defaults to the physical speed of sound due to the high temporal resolution.

2.5 Representation of the Canopy

RAFLES uses explicit canopy information beyond its 3-D leaf area density (LAD) distribution, and additionally includes the stem radius, and 2-D arrays of patch type and canopy top height. Technically, such canopy information can be explicitly measured from aerial and satellite photography (Palace et al. 2008), canopy lidar (Lefsky et al. 2002; Hurtt et al. 2004; Weishampel et al. 2007), and tree sampling (Clark et al. 2008). However, measuring canopy properties at very high resolution over large domains is costly and laborious and, therefore, such information rarely exists. As a realistic surrogate in simulation studies, canopy data are produced with the Virtual-Canopy Generator (V-CaGe), developed by Bohrer et al. (2007). V-CaGe generates fully detailed virtual canopies based on the observed (from the ground or by remote sensing) spatial structure (defined through the spatial autocorrelation function of the observed properties) and structural allometry (defining the empirical relationships between canopy properties) of the forest canopies that are being simulated. In RAFLES, the canopy interacts with the flow field by (1) generating obstacles to the flow resulting from the woody component of the canopy, (2) exchanging heat and moisture and possibly other scalars with the atmosphere, and (3) dragging the flow with the tree leaves.

All open-aperture areas, σ_i, and mesh-cell volumes, Ψ, are computed and stored during the initialization of the model. σ_i and Ψ are reduced wherever hard canopy elements (i.e., tree stems) partially or completely obstruct a grid-cell face, leading to a proportional reduction in any flux across that face:

$$\Psi = \Delta x_1 \Delta x_2 \Delta x_3 - \pi \oint r_{x_3}^2, \tag{19a}$$

$$\begin{cases} \sigma_i = \Delta x_j \Delta x_3 - 2 \int\limits_{x_3 - 0.5\Delta x_3}^{x_3 + 0.5\Delta x_3} r_{x_3} dx_3 & i = \{1, 2\}; i \neq j \\ \sigma_i = \Delta x_1 \Delta x_2 - \max \left| \pi r_{x_3}^2 \right|_{x_3 - 0.5\Delta x_3}^{x_3 + 0.5\Delta x_3} & i = 3 \end{cases} \tag{19b}$$

where r_{x_3} is the vertical profile of stem radius in the cell. The obstacle-induced face reduction is considered to be uniform over the face, as if regulated by a Venetian blind. Similarly, volume reduction of a cell that contains a stem is considered to be uniform, and any mean scalar quantity in the cell remains centred within the full cell. The volume reduction leads to compression of the flow. The force balance between the stem-induced drag and the compression effects determine whether the flow will accelerate or decelerate when moving into a volume reduced grid cell.

In this current version, which is limited to the demonstration of its dynamic component, RAFLES does not resolve a full energy balance to redistribute incoming solar energy in the canopy. Instead, it prescribes sources of moisture (S_q) and heat (S_θ) made consistent with the observed fluxes at the canopy top but redistributed spatially based on the fraction of light interception. To determine the magnitude of these fluxes at each location (horizontally) at the canopy top, the model prescribes a horizontal field of time-constant total fluxes (F), defined as the sum of the spatially averaged latent and sensible heat fluxes. The Bowen ratio (β) and albedo (α), which are horizontally heterogeneous, are derived properties of the virtual canopy (Bohrer et al. 2007).

Following Shaw and Schumann (1992), these prescribed fluxes at the canopy top are distributed vertically through the depth of the canopy, proportional to the amount of attenuated light that is absorbed by each grid cell in a vertical column through the canopy. Assuming light is attenuated exponentially in the vertical direction, a proportionality coefficient (B_{hl}) is defined as follows:

above ground:

$$B_{hl} = \exp\left(-\alpha_x \int_{z_k}^{\text{canopy top}} A_l dz\right) - \exp\left(-\alpha_x \int_{z_{k+1}}^{\text{canopy top}} A_l dz\right), \tag{20a}$$

at ground level:

$$B_{hl} = 1 - \sum_{k=z_2}^{N_{Zcan}} B_{hl_k}, \tag{20b}$$

where A_l is the leaf area per ground area of the canopy at each grid point, k is the vertical grid-layer index, z_1 is the height of the lowest vertical layer in the canopy above ground, N_{Zcan} is the number of vertical layers in the canopy, and α_x is an empirical light extinction coefficient. The sources of moisture and heat in each grid cell are calculated as:

$$S_\theta = \frac{\beta}{(1+\beta)} \frac{B_{hl} F}{\rho c_p \Delta z}, \tag{21a}$$

$$S_q = \left[1 - \frac{\beta}{(1+\beta)}\right] \frac{B_{hl} F}{\rho c_v \Delta z}. \tag{21b}$$

These sources contribute to the potential temperature and moisture, respectively, at each grid point (vertically and horizontally) in the canopy domain, but do not respond to variations in their immediate local environment due to turbulent excursions in temperature and water vapour concentration. Future versions of RAFLES, currently under development, will include multi-layer surface energy parameterization based on the Ecosystem Demography model (Moorcroft et al. 2001; Medvigy et al. 2008) and will also account for hydrodynamic stresses on branches by modelling the water flow through simplified stem-branch systems (Bohrer et al. 2005a).

The total drag force per unit air mass that the canopy and the forest floor exert on the flow, D_c, is comprised of three components: the leaf drag, D_l, which includes skin and viscous drag (Shaw and Schumann 1992; Shaw and Patton 2003), the stem skin drag, D_w, and the soil drag, D_s. They are expressed by the following relationships:

$$D_{li} = -\left(C_{dl} + \frac{1.328}{(R_l)^{1/2}}\right)\left(\frac{A_l \Delta x_1 \Delta x_2}{\Psi}\right)\left|\overline{V}\right|\overline{u_i}, \tag{22a}$$

$$D_{wi} = \begin{cases} -C_{dl}\left(\frac{2(\Delta x_i \Delta x_3 - \sigma_j)}{\Psi}\right)\left|\overline{V}\right|\overline{u_i} & i = \{1,2\};\ j = \{1,2\};\ i \neq j, \\ -C_{dl}\left(\frac{2\sum_j (\Delta x_i \Delta x_j - \sigma_j)}{\Psi}\right)\left|\overline{V}\right|\overline{u_i} & i = 3;\ j = \{1,2\}, \end{cases} \tag{22b}$$

$$D_{si} = \begin{cases} -\left(\frac{\kappa}{\log(\Delta z / Z_{rough})}\right)^2 \left(\frac{\Delta x_1 \Delta x_2}{\Psi}\right)\left|\overline{V}\right|\overline{u_i} & i \neq 3;\ \text{at the lowest grid cell,} \\ 0 & \text{elsewhere,} \end{cases} \tag{22c}$$

where $\left|\overline{V}\right|$ is the wind magnitude (scalar), R_l is the Reynolds number, and C_{dl} is an empirically derived leaf drag coefficient. The bare-soil drag coefficient is parameterized according to Haltiner and Williams (1980), where Z_{rough} is the bare-soil roughness length, and κ is the Von Kármán constant.

2.6 Initial and Boundary Conditions

Due to limits in computational resources, RAFLES was confined to a small spatial domain [$O(1\ \text{km}^3)$] and short time periods (up to a few hours). As with any other limited area model, RAFLES requires initial and boundary conditions. Cyclic boundary conditions are chosen at the lateral sides, assuming that the simulation domain is much larger than the length scale of heterogeneity. A zero-flux condition is set at the top boundary with the vertical velocity specified to be zero and a free-slip condition specified for horizontal velocity. As explained above, Rayleigh friction is applied to the upper five grid levels to reduce reflection (Eq. 3), and at the domain floor, the velocity normal to the floor is specified as no-slip. For initialization, it is assumed that air pressure, potential temperature, humidity, air density and the horizontal components of wind velocity over the simulation domain are horizontally (but not vertically) homogeneous. These initial profiles are taken from nearby radiosonde observations (at the RDU airport, obtained from http://raob.fsl.noaa.gov/) assimilated into a larger scale regional atmospheric model. The initial horizontal velocity profile between 50 and 200 m above ground level is fitted to match the canopy-top observations of the mean wind. This range of heights corresponds to the lower levels of the numerical grid set-up for the RAMS simulations aimed at providing the regional meteorological background. The initial vertical component of wind velocity and SGS TKE are set to zero.

2.7 Output

Full snapshots of the simulation data were saved at 0.5 Hz. Perturbations from time and horizontal-domain averages are calculated and used to evaluate the instantaneous fluxes at a point. For convenience, the 30-min averages of these fluxes at a point are denoted with the operator "$()_t$", and the horizontal-domain averages of these fluxes are denoted with the operator "$()_h$":

$$\overline{(w\varphi)_t} = \overline{\left(\bar{w} - \left\langle\tilde{\bar{w}}\right\rangle\right)\left(\bar{\varphi} - \left\langle\tilde{\bar{\varphi}}\right\rangle\right)}, \tag{23a}$$

$$(w\varphi)_h = \langle (w\varphi)_t \rangle, \tag{23b}$$

$$(\varphi)_h = \langle\widetilde{\bar{\varphi}}\rangle. \tag{23c}$$

At selected locations within the simulation domain, high frequency data were stored for future analyses; these data serve as a spatial sample of 'virtual eddy-flux towers' in the simulation domain and are recorded at 10 Hz, to be consistent with the common sampling

frequency of eddy-covariance systems. Perturbations from the 30-min averages in each cell on these 'virtual towers' are used to calculate 30-min statistics that are then compared to the field-based eddy-covariance flux tower observations. For convenience, perturbations from the 30-min averages at a point (for a virtual or a real tower) are denoted with the operator "$()'_t$", fluxes calculated from these perturbations are denoted with the operator "$()_{tt}$" and the horizontal averages of these fluxes over the 25 'virtual towers' are denoted with the operator "$()_{th}$":

$$(\varphi)'_t = (\overline{\varphi} - \widetilde{\overline{\varphi}}), \tag{24a}$$

$$(w\varphi)_{tt} = \widetilde{(w)'_t\,(\varphi)'_t}, \tag{24b}$$

$$(w\varphi)_{th} = \langle (w\varphi)_{tt} \rangle|_{25\text{ virtual towers}}, \tag{24c}$$

$$(\varphi)_{th} = \langle \widetilde{\varphi} \rangle|_{25\text{ virtual towers}}. \tag{24d}$$

For analysis of the 'virtual tower' data, and eddy-flux tower observations, a rotated coordinate system was used, such that the time-averaged rotated longitudinal wind is aligned with the time-averaged horizontal wind direction,

$$\widetilde{u_r} = \left(\widetilde{\overline{u_1}}^2 + \widetilde{\overline{u_2}}^2\right)^{0.5}. \tag{25}$$

This rotation was applied to both the model and the observed data. The total kinetic energy $\widetilde{TKE}$ includes the resolved and SGS TKE.

The RAFLES' output data are processed using the RAMS Evaluation and Visualization Utilities (REVU) program (Tremback et al. 2004). A modified version of REVU also includes processing options to output the data for stereo, immersed virtual reality visualization using AMIRA or Vis5D+ (Bohrer et al. 2008a).

3 Numerical Experiments

RAFLES' performance is first evaluated using eddy-covariance flux-tower observations collected in a hardwood canopy during typical convective days in the spring and winter. These two seasons represent the two end-members in terms of canopy structure and expected large-scale eddy sizes within the entire ABL.

3.1 Simulation Set-up

Two simulations were conducted, forced by the mesoscale and canopy state conditions on December 17, 2001 and April 4, 2002. Runs around noontime were used because of the near stationarity in the near-vertical penetration of the incident solar radiation. Hereafter, these two simulation runs are referred to as the "winter" and the "spring" simulations, respectively. The sensible heat flux is not small in both cases, suggesting significant contribution from buoyant production to the turbulent kinetic energy (Table 1). Initial conditions were first generated with the RAMS model (Version 4.4) configured with four nested grids: a low-resolution grid ($64 \times 64\,\text{km}^2$) over the eastern and central USA and a high-resolution grid ($1 \times 1\,\text{km}^2$) over the Duke forest (near Durham, North Carolina). Two more grids at intermediate resolutions were used to provide a transition from the low to the high resolutions. Accordingly, mesoscale meteorological conditions corresponding to the location and timing are used to force RAMS (NCEP re-analysis dataset, Kalnay et al. 1996). For these two runs,

Table 1 Canopy structure parameters and atmospheric forcing

Canopy parameter	Winter canopy			Spring canopy		
	Heterogeneous	Patchy		Heterogeneous	Patchy	
		Forest	Gap		Forest	Gap
Stand density (stems ha^{-1})	937	937	0	937	937	0
Mean canopy height (m)	24.06	24.06	0.3	24.06	31.98	0.3
Std of canopy height	3.79	3.79	0.05	3.79	3.79	0.05
Mean LAI ($m^2 m^{-2}$)	1.37	1.37	0.5	2.95	2.95	0.5
Std of LAI	0.14	0.14	0.1	0.26	0.26	0.1
Mean Bowen ratio	15.25	15.25	12.60	1.25	1.25	2.72
Std of Bowen ratio	0.25	0.25	0.08	0.16	0.16	0.08
Mean canopy-top total flux forcing ($W m^{-2}$)	225	232	202	324	365	307
Observed canopy-top mean u_r ($m s^{-1}$)	2.5	2.5	2.5	0.5	0.5	0.5
Std of canopy-top total flux	0	10.0	1.0	0	10.0	1.0
Length scale of canopy height heterogeneity (m)	6.5	6.5	0.5	6.5	6.5	0.5

In the patchy simulations, 30 m was used as the landscape-level length scale, which determines the spatial distribution of grassy gaps within the forested domain

spring atmospheric conditions were warmer and dryer, the ABL thicker, and the horizontal winds weaker than during the winter run. The spatially-averaged sensible and latent heat fluxes were obtained from the meteorological tower within the Duke forest hardwood stand (for a description of the flux dataset, see Stoy et al. 2006). The fluxes are prescribed inside the canopy according to Eqs. 20–21.

The virtual canopies required for the simulations were generated with V-CaGe (Bohrer et al. 2007), based on local canopy observations collected within the Blackwood Division of the Duke Forest. The spatial structure used by V-CaGe to represent the canopy was prescribed as a negative exponential relationship with an *e*-folding length of 6.5 m, defined as the typical length scale of the canopy structure. It is based on an averaged and smoothed autocorrelation function derived from the distribution of canopy heights at the Duke Forest derived from stereoscopic airborne images. The landscape length scale used in V-CaGe to generate the distribution of land-surface patches, which determined the typical size and spatial distribution of the gaps in the patchy simulations, was 30 m. Other canopy properties based on site specific empirical data included: stand density, mean and standard deviation of canopy top height, and normalized vertical LAD profile (Schäfer 2002; McCarthy et al. 2007). Also, the empirical relationship between height and stem diameter at breast height was obtained from Naidu et al. (1998). As indicated in Table 1, the differences between the canopy structures consisted of denser foliage and a lower mean Bowen ratio in the spring canopy relative to the winter canopy. Total canopy-flux forcing is stronger in the spring, split almost equally between latent and sensible heat fluxes. During the winter, the fluxes are weaker and the mean Bowen ratio is 15 given the low foliage and humidity conditions (Table 1; Fig. 1).

As illustrated in Fig. 1, two canopy structures were simulated under both spring and winter conditions: (i) A natural canopy with a dominant length scale of heterogeneity, $r_h = 6.53$ m (the mean radius of a tree crown), representing observed tree-level microscale heterogeneity.

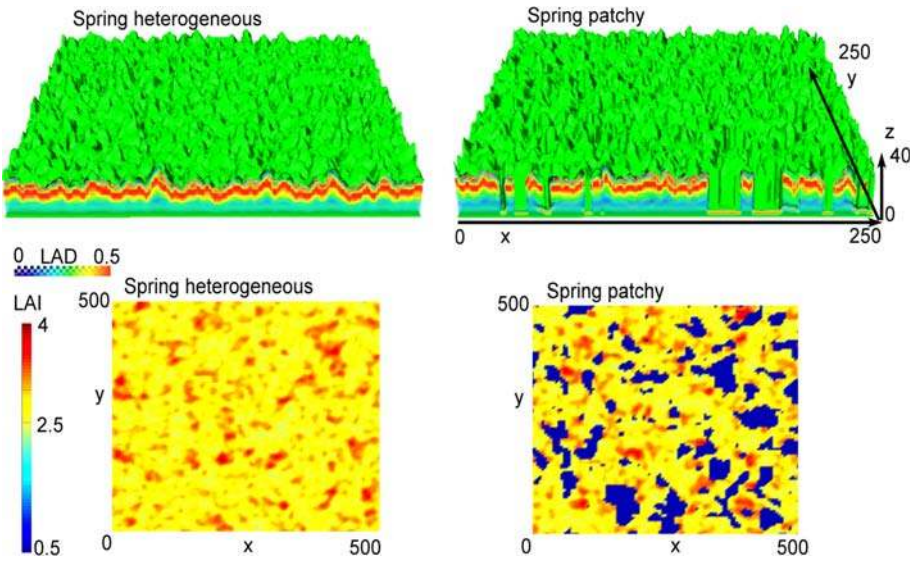

Fig. 1 Simulated canopies in the spring case. The 3-D rendering in the upper row illustrates the canopy-top height (*green surface*) and leaf area density (LAD) (m^2 leaf m^{-3} air) (*colour*). The *lower row* presents the leaf area index (LAI). The domain dimensions are in m. The illustrations represent sub-sections of the simulation domains (dimensions shown on axes in m)

The sum of the vegetation-to-air sensible and latent heat fluxes is assumed to be horizontally homogeneous in this case. This naturally heterogeneous canopy, hereafter referred to as the "reference" case, was also used for model evaluation; (ii) A patchy canopy, which consists of the same, naturally heterogeneous canopy as in (i) but interspersed with grassy patches and normalized such that the mean canopy properties (height, LAI, total flux) are be the same in both (i) and (ii). In the patchy canopy, grassy patches covered 20% of the ground area. The forested patches in this stand have a larger sum of the vegetation-to-air sensible and latent heat fluxes, with small spatial heterogeneity, which is correlated with canopy top height. The relative values of the fluxes at the grassy patches are based on measurements in an open field at the same site (for a description of the grass-site flux dataset, see Novick et al. 2004). Table 1 provides relevant canopy and flux characteristics needed for the simulations in both cases. The simulation cases are denoted as: HW, HS, PW, PS, for the heterogeneous canopy in the winter, and spring, and patchy canopy in the winter, and spring, respectively.

Several of the parameters that need to be assigned for the simulations are still not well known; most pertinent is the leaf skin drag coefficient, C_{dl}, whose range is between 0.1 and 0.3 (Shaw and Patton 2003; Katul et al. 2004). To identify whether the optimum value is bounded by this logical range, the sensitivity of the model to this parameter was carried out. Four simulations were performed for each season, each using a different C_{dl} value. Based on a comparison of the simulated $(u_r)_{th}$ at 39.8 m, corresponding to the height of the tower-top sonic anemometer at Duke Forest, the optimum $C_{dl} = 0.15$, which is identical to the value found by Katul et al. (2004) best match a k–ε model calculations conducted for a similar southern hardwood canopy experiment presented in Meyers and Baldocchi (1991).

The LES horizontal domain consists of 256× 256 grid cells, $5 \times 5\,m^2$ each. In the vertical, the grid consists of 98 elements, with a constant spacing of 3 m from the ground surface up to twice the mean canopy height. Above that height, the spacing is stretched by a factor of

1.1 from element to element up to a maximum spacing of 30 m. This resulted in a simulation domain size of 1,280 × 1,280 × 1,414 m^3. The frequency for the long time-step is set to 20 Hz, while the frequencies for the nested timesteps, $1/\Delta t_m$ and $1/\Delta t_s$, are set to 40 and 160 Hz, respectively. The data output frequency is set to 0.5 Hz for storage purposes, and, as mentioned earlier, high frequency (10 Hz) data are also recorded from 25 columns, equally spaced throughout the simulation domain.

The simulations commenced with the resolved TKE = 0, then the domain-averaged TKE evolved rapidly during the first 20 min of the simulation, and continued to gradually increase throughout the whole period of the simulation due to the constant noontime radiative heating imposed in the simulation and the periodic boundary conditions. The 30-min period following the first 2.5 h into the simulation was selected because, during this period, the effects of the initial conditions on the mean resolved TKE were negligible, and the domain-averaged resolved TKE was close to stationary.

3.2 Observations

The atmospheric variables necessary to compute turbulent fluxes were measured on a meteorological tower situated in a second-growth 80–100 year old oak-hickory forest within the Blackwood Division of the Duke Forest, near Durham, North Carolina. The tallest tree adjacent to the tower was 36 m tall and the mean canopy height of the surrounding forest was 24.1 m. Three sonic anemometers, mounted on this tower at 18, 30, and 39.8 m above the forest floor, sampled simultaneously the three velocity components at a frequency of 10 Hz. Four 30-min periods (from 1100 to 1300 local time) were used to evaluate the model performance around noon. This period was selected because scalar fluxes are near their maximum and the light attenuation model is likely to perform best when the radiation beam penetrating the canopy is almost vertical. For each of these periods, the 30-min averaged $\widetilde{u_r}$, $(TKE)_{tt}$, $(uw)_{tt}$ and $(u_r w)_{tt}$ (see Eqs. 24–25 for definitions) were calculated. The average and range of these four 30-min averages were used for evaluation of the model results.

3.3 Comparison Between Observations and RAFLES

The simulations here did not account explicitly for the specific microscale variability around the meteorological tower. Instead, the microscale variability was generated using a virtual canopy constructed from the statistics of the real canopy properties using data from the entire site. Therefore, the location of the eddy-flux tower was also not explicitly represented as a single location in the simulation domain. Hence, the agreements between observations and simulation data are not compared in a one-to-one fashion based on the location. Data from the four observed 30-min periods were compared to simulation results from 25 equally spaced horizontal locations throughout the simulation domain, at the heights where the sonic anemometers were installed. Simulation results where considered acceptable if the range (mean ± standard deviation) of the simulated results overlapped the range of the four mean observed values at the corresponding height.

Figure 2 shows the comparison for both spring and winter runs between 30-min time-averaged observations, $\widetilde{u_r}$, and RAFLES-modelled, time-averaged, streamwise rotated, horizontal velocity, averaged over the 25 virtual towers where model data were available at high frequency in the simulation domain, $(u_r)_{th}$. As has been observed in other forests (Launiainen et al. 2007; Su et al. 2008), the model resolved a weak (difference of 0.1–0.3 $m\,s^{-1}$) secondary wind-speed maximum between the tree crowns and the understorey, where the LAD is minimal. This local maximum was not present in the winter simulation when the

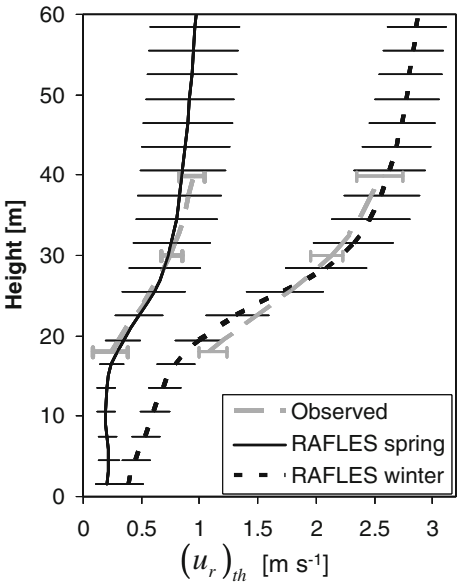

Fig. 2 Mean vertical profiles of longitudinal velocity, $(u_r)_{th}$ (see Eqs. 24–25), in and above the canopy simulated in the reference cases for the spring and winter. Each profile represents the average of 10 Hz sample frequency of velocity, over 30 min of simulation, at 25 locations in the virtual domain. *Open error bars* for RAFLES simulation data represent one standard deviation. *Closed error bars* for observations represent the maximum and minimum between four 30-min periods around noontime

canopy was much sparser and winds stronger. In the winter simulation, the observed velocity gradient between the canopy top and the lowest sonic level (18 m) was slightly smaller than the simulated gradient, but the opposite was true in the spring. Yet, these differences were still smaller than the observed range.

As depicted in Fig. 3, simulated momentum fluxes were within the range of observed values in the spring simulation. The vertical profiles of $(TKE)_{th}$, $(ww)_{th}$, and $(u_r w)_{th}$, (see Eqs. 24–25 for definitions) were within the observed range, and in the winter simulation, $(TKE)_{th}$ and $(ww)_{th}$ were lower than observed, but this difference was again not significant. The observed $(u_r w)_{th}$ was lower (i.e., less negative) than the simulated one. In the winter, TKE above the canopy is largely produced by shear, unlike the strongly convective spring case where buoyancy contributed more to TKE production at this height. As in Dwyer et al. (1997), the TKE generated by the strong vertical shear due to the drag with canopy elements, is the major term contributing to TKE production in the upper part of the canopy and just above it, and it is characterized by a shorter integral length than TKE produced by convection. Indeed, in the winter cases the integral length scales for vertical velocity (55–65 m) were only about half the value of the spring cases (100–115 m, in the patchy and reference canopies respectively, Table 2). The integral length scale of vertical velocity was assumed to be the lag distance over which the mean autocorrelation first crossed zero.

The resolution of smaller eddies is more sensitive to the model's grid resolution and to the SGS parameterization, and it is reasonable to assume that improved SGS parameterizations would improve the model performance in high-shear conditions (e.g., Bou-Zeid et al. 2008; Stoll and Porte-Agel 2008; Yue et al. 2008).

Figure 4 shows the power spectra of the three wind velocity components at several heights within and above the canopy. At a range of length scales from 800 m to about 80 m these spectra do scale with an exponent of –5/3 above the canopy. Given that these scales are much larger than the fine scales in the sense of Kolmogorov's theory, the onset of a –5/3 power law here is likely to be due to the convective nature of the large eddies. It is well known that for the neutrally buoyant boundary layer the velocity and temperature spectra scale as –5/3 within

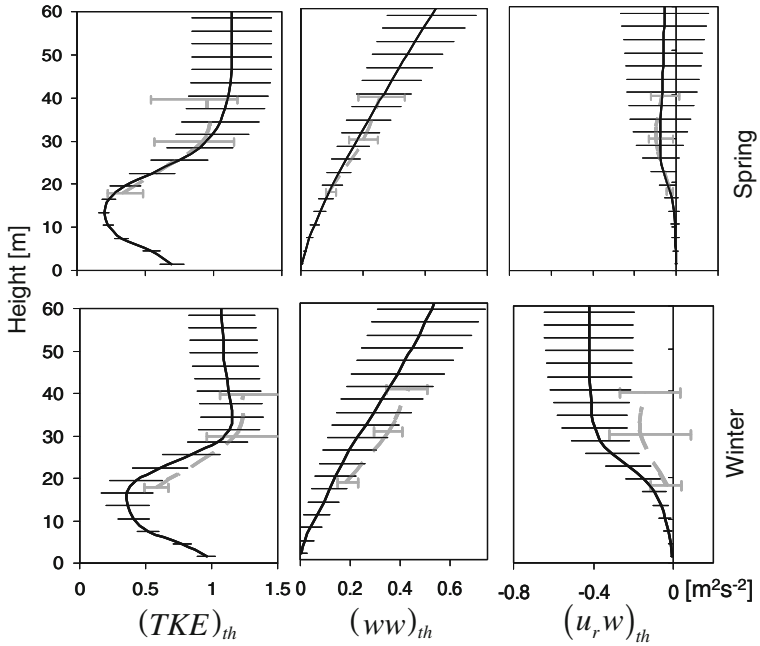

Fig. 3 Same as in Fig. 2 but for total kinetic energy, $(TKE)_{th}$, vertical velocity variance, $(ww)_{th}$, and momentum flux, $(u_r w)_{th}$

the inertial subrange (but not at larger scales), however, for the purely convective boundary layer, the –5/3 power-law scaling extends to larger length scales beyond the inertial subrange (Katul et al. 1995). Theoretically, a numerical mesh at a spacing of Δx can correctly represent a wave with a wavelength equal to or larger than $2\Delta x$. However, in numerical simulations with discrete grid spacing, conversion of TKE from the resolved scales to the SGS leads to velocity power spectra that are not accurately resolved up to an order of $10\Delta x$ (see Chow et al. 2005). The within-canopy spectra E_u and E_v are slightly steeper at the higher part of the well-resolved range (800–100 m) than the spectra at the open boundary layer, which follow the $-5/3$ slope at this range. Inside the canopy, energy short-circuiting within the canopy is expected to yield a slightly steeper slope than $-5/3$. A secondary peak in the within-canopy spectra is produced at the small scales (Cava and Katul 2008) but these are smaller than $2\Delta x$ and, therefore, a secondary peak is not expected to be apparent in the simulated resolved power spectra.

Introducing the SGS backscatter scheme of Bhushan and Warsi (2005) into RAFLES improved this unavoidable deficiency, as compared to the Deardorff (1980) scheme that has been adopted by many LES models (e.g., Shaw and Patton 2003), including RAMS (Hadfield et al. 1991; Avissar et al. 1998). The Deardorff (1980) scheme was chosen because of its simplicity, numerical efficiency, and realistic behaviour when implemented in the parent model RAMS. A method, which was adopted in a previous study (e.g., Su et al. 1998), to remedy this deficiency consisted of adjusting some of the coefficients of the SGS scheme in the canopy layers. Given the small grid size used here, it is assumed that the within-canopy SGS errors are minimized and no empirical correction was made to the SGS-TKE parameterization. The backscatter improves the scaling of turbulence, particularly at the intermediate range of scales (Bhushan and Warsi 2005).

Table 2 Effective surface parameters and fluxes from the different canopy structures in the spring and winter simulation conditions

	Winter canopy		Spring canopy	
	Heterogeneous	Patchy	Heterogeneous	Patchy
$(l_m)_s$ (m)	61.09	59.44	70.58	45.25
δ_e	18.09	17.29	15.69	21.10
dl_m/dz	0.449	0.422	0.542	0.578
$(L)_s$ (m)	−150.63	−107.52	−13.14	−20.34
ε	−0.34	−0.42	−4.80	−2.51
z_{0m} (m)	3.19	2.52	1.64	2.11
h_d (m)	16.68	13.85	16.74	18.53
u_{*s} (m s^{-1})	0.65	0.58	0.30	0.34
h_e (m)	24.2	21.7	24.3	27.1
h_s (m)	61.0	59.4	70.6	45.25
$h\|_{(\Delta S0=0)}$	62.04	39.42	60.36	37.62
$(u_r w)_{th}\|_{II/IV}/(u_r w)_{th}$	0.58	0.57	0.88	0.84
Integral length scale for w (m)	65	55	115	100

Some of these parameters were derived from the fields of the resolved model results using Monin–Obukhov similarity theory. l_m is the effective mixing length for momentum transport, and dl_m/dz its vertical gradient, δ_e is penetration depth, $L = u^{*3}(\theta_v)_h/kg((w\theta_v)_h)_s$ is the Obukhov length, $\varepsilon = (h_s/L)_s$ is the ABL stability parameter, z_{0m} is the roughness length, u_* is friction velocity, h_d is displacement height, h_e is the effective mean aerodynamic canopy height, h_s is the effective surface-layer depth, and subscript s denote values at this surface-layer depth. $h|_{(\Delta S0=0)}$ is the height at which the difference between stress fraction due to ejections and sweeps ΔS_0 changes sign. $(u_r w)_{th}|_{II/IV}/(u_r w)_{th}$ represents the fraction due to ejections or sweeps (quadrants IV and II, respectively) of the total momentum flux exchange between the canopy and ABL (evaluated at h_s). This was evaluated from the 25 high-frequency data columns using quadrant analysis. Integral length scale for w was calculated at h_e

Wake generation by elements in the canopy (i.e. leaves, stems, branches, and branch-leaf clusters) is known to have a major contribution to the production of TKE inside the canopy (Meyers and Baldocchi 1991; Poggi et al. 2004a; Cava and Katul 2008). Wake eddies are typically smaller than the resolution used here, and therefore contribute to SGS TKE and will not contribute to the power spectra of the resolved velocity components. Shaw and Patton (2003) suggested a parameterization that includes wake generation by canopy elements, but this was not implemented in the current version of RAFLES because it is dependent on an empirical "wake generation length scale". In the case of uniform isolated rods or stems with a diameter distribution possessing a clear mode, the wake generation length scale is related to the rod or stem diameter (Poggi et al. 2004b; Poggi and Katul 2006; Cava and Katul 2008). However, this length scale becomes ill defined for the composite case of leaves and branches, and is likely to be influenced by leaf clumping and stem-branch structure and, to date, cannot be readily inferred from canopy geometry in heterogeneous canopies.

4 Effects of Tree-Scale Canopy Heterogeneity

The effects of tree-scale canopy heterogeneity on the flow field can be explored in a number of ways and using several statistical measures. As a logical starting point here, the tree-scale

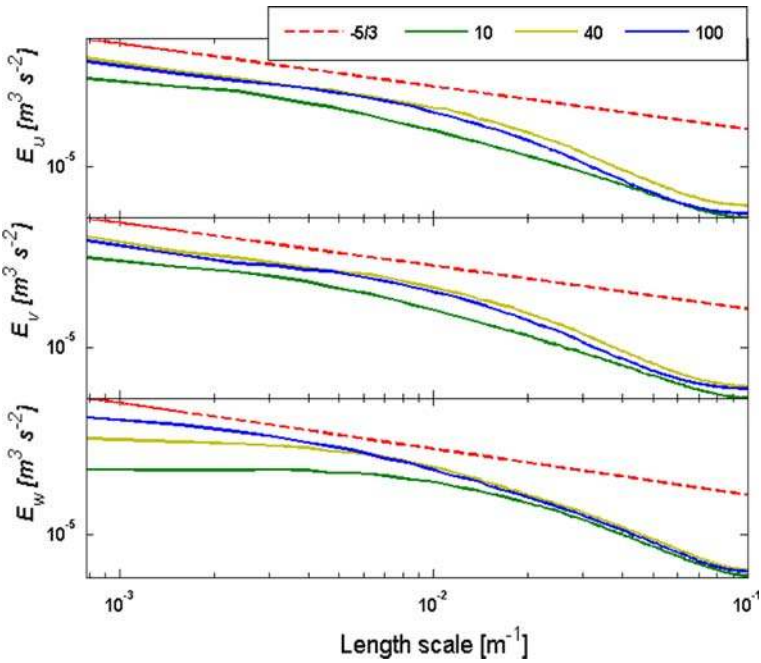

Fig. 4 Power spectra of the three velocity components (E_u, E_v, E_w) in the reference spring simulation at various heights above the forest floor (indicated at the legend in m above ground). The effective mean aerodynamic canopy height at that simulation was $h_e = 24.3$, the boundary-layer depth = 400 m. The $-5/3$ power law line (*dashed, red*) is the expected slope in the inertial sub-range (K41 theory) and it is shown for reference. The *dark green lines* represent spectra from inside the canopy, *light-green spectra* are from the model layer just above the tallest canopy element in the domain, and the *blue lines* are from the boundary layer, above the roughness sublayer (see Table 2)

canopy heterogeneity effects are explored at three levels. The first level considers the effect of tree-scale heterogeneity on the common representation of the canopy via length scales (i.e. zero-dimensional representation of the 3-D canopy) such as the zero-plane displacement, the aerodynamic roughness length, the surface-layer depth, and the so-called penetration depth. These length scales are used in mesoscale and large-scale atmospheric models to represent the effects of the 3-D structure of the canopy on momentum transfer via a 'scalar' quantity applied through the boundary condition to the bottom atmospheric layer. The second level considers the normalized horizontally-averaged profiles of the first and second moments of the flow, where the normalization is based on the horizontally-averaged fluxes in the surface layer (i.e. the effects of the canopy heterogeneity on one-dimensional canopy models). This comparison permits assessment of how the tree-scale heterogeneity disturbs the entire spatially-averaged profiles from their canonical (and well-studied planar-homogeneous) values inside the canopy and in the surface layer. The third level considers the effects of such tree-scale heterogeneity on the spatial variability of the ejection-sweep cycle and its propagation to momentum and mass fluxes. Eddies that contribute to the ejection-sweep cycle are also the flux-transporting eddies of mass and momentum.

4.1 Level 1: Canopy Representation Via Similarity Theory and Length Scales

In large-scale atmospheric models, the 3-D effects of the canopy on the flow are often represented via, for example, the aerodynamic roughness length and zero-plane displacement, and

coupled to the atmosphere using Monin and Obukhov similarity theory (MOST) or analogous formulations.

An effective surface-layer depth, h_s, is defined as the minimal distance above ground and within the atmospheric surface layer such that the vertical gradient of the Obukhov length (see Table 2 for definition), dL/dz, is approximately zero, i.e. quasi-constant fluxes of heat and momentum, a key assumption of MOST. For convenience, we denote the surface fluxes, i.e., horizontally-averaged fluxes at h_s, with a subscript "s".

The aerodynamically effective height of the canopy top, h_e, was determined from the model results as the height of the inflection point in $\langle \widetilde{u_r} \rangle$ (Raupach et al. 1996). The use of aerodynamic canopy height as a reliable scaling variable in heterogeneous canopies was recently confirmed in a study by Nakai et al. (2008). The displacement height, h_d, was computed from the centroid of the drag force exerted by the vegetation on the air flow (Jackson 1981). The roughness length, z_{0m}, was determined by a least-squares optimization within the surface layer of the MOST-driven relationship between mean velocity and height above h_d using classical stability correction functions for an unstable atmosphere. Penetration depth, δ_e, is a length scale describing the vertical distance from the top of the canopy influenced by changes in turbulent mixing. It is defined as the distance between h_e and the location where $(u_r w)_h = 0.1(u_r w)_h|_{h_e}$(Nepf et al. 2007), and will be used as a scalar measure for Reynolds stress profile comparisons.

Alternatively, quadrant analysis can be used for defining different exchange regimes within and above the canopy (Thomas and Foken 2007). Quadrant analysis refers to the joint scatter across four quadrants defined by a Cartesian plane whose abscissa is $(u_r)'_t$ and ordinate is $(w)'_t$. The four quadrants are connected with four modes of momentum transfer: events in quadrant II ($(u_r)'_t < 0, (w)'_t > 0$) and quadrant IV ($(u_r)'_t > 0, (w)'_t < 0$) are called ejections and sweeps respectively; events in quadrant I ($(u_r)'_t > 0, (w)'_t > 0$) and quadrant III ($(u_r)'_t < 0, (w)'_t < 0$) are called outward and inward interactions, respectively. Typically, ΔS_0, the difference between the stress fraction due to ejections (measured as the mean flux contributions of events when the flux is in quadrant II) and sweeps (flux contribution from events in quadrant IV), can be used to fingerprint the transition from canopy flows to surface-layer flows (Katul et al. 1997, 2006). We define $h|_{(\Delta S0=0)}$ as the height at which ΔS_0 changes sign thereby marking a shift in the ejection-sweep cycle properties.

For reference, it is well known that inside a dense canopy and extending to within the canopy sublayer, sweeps dominate momentum transfer for neutral flows (i.e. Poggi et al. 2004a,b,c). For sparse canopies, ejections can dominate within the canopy as well. As the surface layer is approached, ejections become the dominant mode of momentum transfer [see discussion in Katul et al. (2006) regarding the connection between ΔSo, higher-order cumulants, gradients in second-order statistics, and the definition of the canopy sublayer]. We calculated this height based on the simulation data from the 25 sample locations where we saved high-frequency data in each simulation.

Integral length scales of vertical velocity, most pertinent to vertical material exchange between the biosphere and atmosphere, were calculated for lags increasing by Δx over each row and by Δy over each column (separately) of a full domain snapshot. A separate snapshot was used every 60 simulated minutes. All the resulting autocorrelation profiles were averaged according to lag distance.

Table 2 lists these resolved length scales in the different simulation cases. When compared to the homogeneous case, canopy-top heterogeneity decreased the displacement height and increased the roughness length and penetration depth. This effect was stronger in the spring, when the tree canopy was densely populated with foliage (as expected). Compared with the heterogeneous cases, the patchy canopy showed further increases in displacement height and

penetration depth in the spring but minor changes in the winter. In both seasons, the integral length was reduced in the patchy cases by about 15% (Table 2). During the spring, the contrast between gap-openings (full penetration) and full canopy cover (low penetration) is much more pronounced, allowing for enhanced mean penetration across the entire domain. There was no clear difference between the spring and winter simulations in $h|_{(\Delta S0=0)}$. In both cases, the patchy canopy had a much lower mean $h|_{(\Delta S0=0)}$ indicating a shallower roughness sublayer (when defined as such). As earlier noted, within the canopy, sweeps dominate but in sparser or open areas, ejections are likely to dominate and, hence, reduce the area-averaged $h|_{(\Delta S0=0)}$. Interestingly, $h|_{(\Delta S0=0)}$ also varied from 1.5 to 3 times the canopy height, indicative of the thickness of the roughness sublayer. These results suggest that the fractional area of gaps may be a logical choice for a scaling variable to adjust the displacement height, roughness length, and penetration depth even for heterogeneous canopies.

4.2 Level 2: Canonical Profiles Inside the Canopy

Figure 5 presents the vertical profiles of the mean sensible and latent heat fluxes, $(wt)_h$, $(wq)_h$, mean rotated horizontal streamwise velocity, $\widetilde{\langle u_r \rangle}$, vertical velocity standard deviation, $(ww)_h^{0.5}$, and momentum fluxes, $(u_r w)_h$. The effective mixing length for momentum transport, l_m, is also shown and is computed as $l_m^2 = -(u_r w)_h / \widetilde{\langle \partial u_r / \partial z \rangle}^2$.

From Fig. 5, the differences between these mean profiles in heterogeneous and patchy canopies are minor after normalizing with the aerodynamically effective height and surface-layer fluxes (including the friction velocity u_{*s}). These results are encouraging because they do demonstrate that the aerodynamic height is an appropriate scaling variable for inhomogeneous canopies. Moreover, the microscale heterogeneities, being statistically homogeneous in the plane parallel to the ground and occurring on length scales much smaller than the domain size, do not appreciably alter the vertical distribution of turbulent fluxes, provided the absolute flux differences are accounted for in the surface layer (usually the upper boundary condition imposed on the canopy sublayer).

The effective mixing length has a small local maximum value inside the canopy consistent with numerous canopy turbulence studies (Wilson and Shaw 1977; Katul and Chang 1999; Poggi et al. 2004a). This characteristic of the vertical profile of l_m was predicted from analytical analysis by Harman and Finnigan (2007). However, dl_m/dz is affected by surface heterogeneity and surface heating, and in a neutrally buoyant ABL above a homogeneous surface is equal to the von Kármán constant. Indeed, dl_m/dz was 0.45 and 0.44 for the HW and PW cases (i.e., winter cases, when conditions are closer to neutral), above the effective surface-layer depth. However, $dl_m/dz = 0.54$ and 0.58 in the more convective HS and PS cases, respectively (as expected). Depending on the simulation case and the height from the ground, l_m near the canopy top and inside the canopy was between $0.3h_c$ and $1.1h_c$. This length scale is equivalent to the crown size, indicating that heterogeneity at this scale of individual tree crowns has an impact on the local flow dynamics.

4.3 Level 3: Effects of Tree-Scale Heterogeneity on the Spatial Distribution of Fluxes

The height of the roughness sublayer, where the effects of surface features are still persistent, extends from the canopy top to 2–5 times the canopy height (Raupach and Thom 1981). The effects of tree-scale canopy heterogeneity on the spatial distribution of the ejection-sweep cycle, and their concomitant effects on the flux distribution inside the canopy roughness sublayer are explored here. The relationship between the spatial patterns of fluxes and the

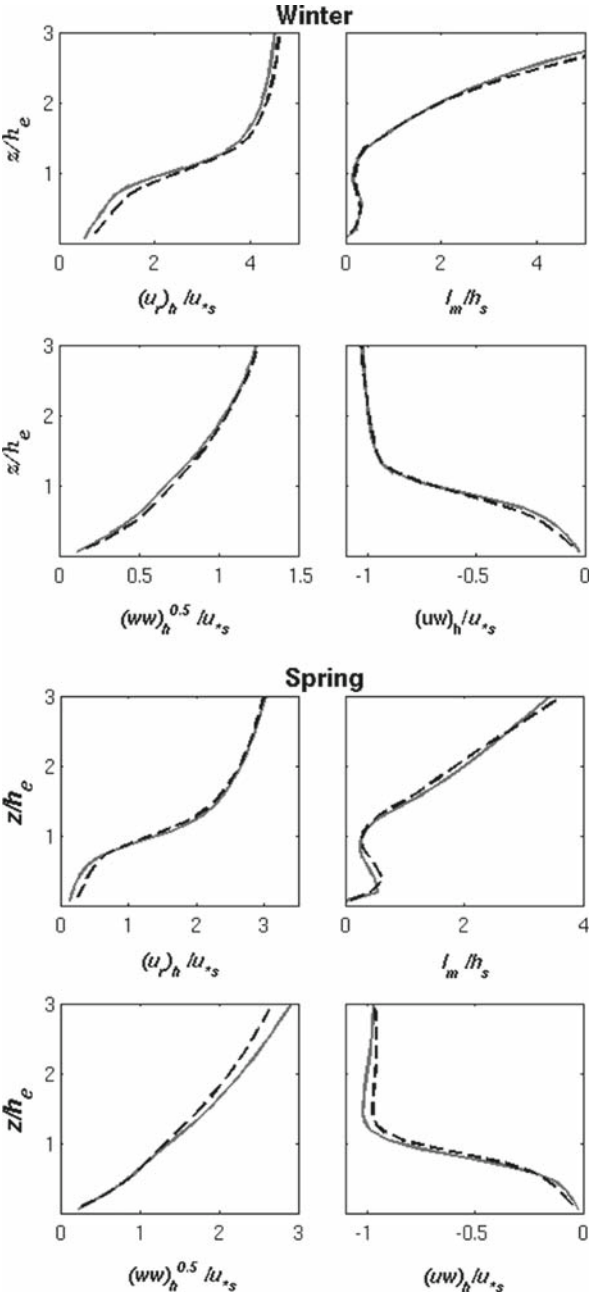

Fig. 5 Normalized and dimensionless vertical profiles of mean momentum fluxes, horizontal wind speed and effective mixing length. *Bold, shaded lines* mark the reference canopy; *dashed, black lines* mark the patchy canopy. The values of the aerodynamic effective canopy height, h_e, used for normalization of the vertical axis, and h_s, u_{*s}, (the effective surface heights, and the friction velocity at h_s, respectively), which were used for normalization of the profile, are presented in Table 2. l_m is the mixing length, $(ww)_{th}^{0.5}$ is the standard deviation of vertical velocity, $(uw)_{th}$ is the momentum flux (see Eqs. 23–25 for averaging notation)

canopy structure was analyzed in the following way: first, the time-averaged covariances of the perturbations from the time and horizontal domain average, $(w\varphi)_t$ (Eq. 23a), were calculated for each variable in the simulation domain. The model-resolved covariances are analyzed using conditional analysis based on the sign of the vertical velocity. Three cases of the spatial patterns of the fluxes are compared: the reference case is the time-averaged flux, the second case is the conditional time-averaged flux in updrafts characterized by $w > 0$,

and the third, is the conditional time-averaged flux in downdrafts characterized by $w < 0$. We calculated each of these time-averaged covariances at a unique coordinate i, j, k (for the longitudinal, latitudinal, and vertical coordinates, respectively) in the simulation domain. All the data points that are at the same height (i.e., share the same k coordinate) define a single set, or layer, of covariance data. Next, the canopy-top height in each horizontal location $(i; j)$ was calculated from the maximal height within that location that included leaves. Finally, for each horizontal layer of covariance data separately, we tested the correlation between the covariance and canopy-top heights, matching each canopy-top-height data point with the corresponding covariance data point (same i, j location). We used the correlation coefficient from the quadratic fit between these two variables, resulting in $3N_k$ correlation plots (where $N_k = 98$ is the number of vertical grid layers in the simulation domain) per covariance variable, $(w\varphi)_t$. Each of these correlation coefficients may be affected by spurious correlations between the surface features and eddy structure due to aliasing of dominant length scales, and so the significance of these correlations is tested by the usual randomization and false-detection technique. One thousand virtual randomized canopies were generated for each simulation case using V-CaGe, and the locations of canopy features were randomized by drawing an independent random phase (with a uniform distribution between $\pm\pi$) in wave space during the construction of these randomized canopies (using fast Fourier transform), while keeping all other properties of the randomized canopy identical to the canopy used for the simulation case (see Bohrer et al. 2007). Correlation coefficients between these 2-D flux fields computed by RAFLES for the canopy structures in Fig. 1 and the canopy heights from each of the 1,000 randomized canopies were computed. Correlations were considered significant if less than 5% of the randomized canopies had a higher correlation coefficient than those obtained from the correlation between the flux fields in each simulation case and the canopy height in the actual canopy used to generate the fluxes from the LES simulation case. The analysis was conducted for the bottom 34 vertical layers, between 1.5 and 102 m above ground level, i.e. $0.1h_c$–$4h_c$. At each layer, the horizontal domain contains 253×253 non-boundary points. The method demonstrated here for measuring the significance of the correlation between fluxes and the canopy height can also be used to effectively determine the thickness of the canopy roughness sublayer (for heterogeneous cases).

Despite the overall similarity in normalized canonical profiles between the two canopy structures, the spatial details of the wind speed and vertical fluxes inside and above heterogeneous canopies are affected by the canopy structure. Figure 6 shows the vertical profiles of the spatial correlation coefficients between momentum or scalar fluxes and the canopy-top height. We found that $(ww)_t$ in updrafts is strongly and negatively correlated with canopy top-height, indicating stronger and more frequent ejection events occurring over shorter trees. Prabha et al. (2007) showed that boundary-attached rolls can form along heat-flux maxima, when the length scale of heterogeneity is smaller than the boundary-layer depth, depending on the boundary-layer stability, geostrophic wind and the orientation of the patterns of heterogeneity to the mean wind direction, and up to a mean difference of 15–20% between point observations at the attached role location and at other locations in the domain. We found similar effects of an attached circulation over much smaller scales, and particularly over shorter trees surrounded by taller ones. An illustration of this effect of canopy structure on ejections and sweeps is presented in Fig. 7.

Close to the ground, $(ww)_t$ in downdrafts is strongly and positively correlated with canopy-top height for all cases ($r^2 > 0.6$). Just above the mean canopy height, $(ww)_t$ is strongly and negatively correlated with the canopy height (Fig. 8). This shift from positive to negative correlation illustrates a transition between the lower region inside the canopy, deeper than the eddy-penetration depth, which is dominated by the local circulation (Fig. 7b), and

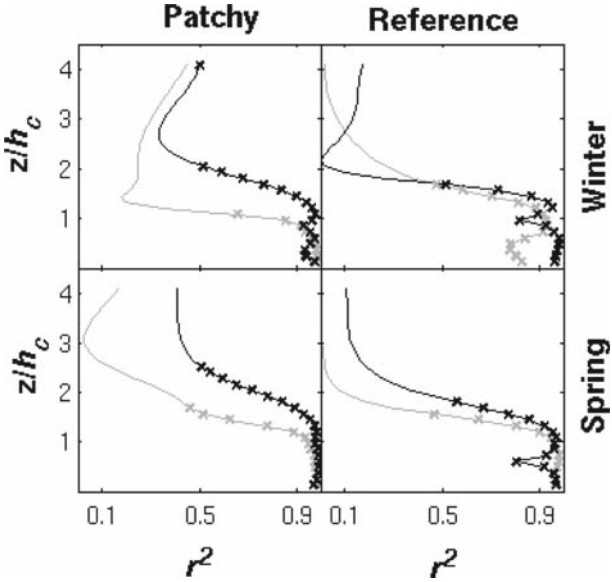

Fig. 6 Vertical profiles of the r^2 of the second-order polynomial correlation between $(ww)_t|_{w>0}$ (updrafts, *grey lines*) or $(ww)_t|_{w<0}$ (downdrafts, *black lines*) and canopy-top height at the four simulation cases. Heights where these correlations are significant are marked by x

the upper region of the canopy that is directly affected by larger eddies penetrating from above (see Fig. 7 in Poggi et al. 2004c). A snapshot, 15 min into the simulation (Fig. 8), illustrates the vertical wind velocity in each simulation case along a horizontal full-domain cross-section. These variations in the vertical wind velocity are indicative of a topology of eddy structures. The details of the correlations between $(ww)_t$ and canopy-top height at three heights are presented in Fig. 9, where the quadratic shape of the relationships indicates that the maximal effects are concentrated in locations where the canopy is relatively short (i.e., short trees and gaps) and above the tallest trees in the domain. The relative flux contribution of structures responsible for the sweep-ejection cycle was calculated as the ratio between the vertical flux from events in quadrants II and IV, and the total vertical flux. Surprisingly, the relative contribution of ejection and sweeps was similar between patchy and heterogeneous simulations, despite being very different between spring and winter simulations (0.58, 0.57, 0.88, 0.84 in HW, PW, HS, PS respectively, Table 2). This indicates that the planar average number and importance of ejections and sweeps is not affected by canopy structure, while the spatial distribution of their locations within the planar domain is affected by small-scale canopy heterogeneity.

Consistent patterns emerge from these vertical profiles (Fig. 7), and the correlation is always significant inside the canopy. In the reference canopy (spring and winter heterogeneous cases) the momentum flux becomes decoupled from the canopy structure (i.e. the correlation with canopy height becomes less significant) between 1 and 2 times the height of the canopy top. Counterintuitively, the vertical momentum flux in updrafts is also somewhat decoupled at the same height or closer to the canopy than the flux in downdrafts. In the PW case a range of significant correlations for $(ww)_t$ in downdrafts emerges around $4h_c$.

Raupach and Thom (1981) determined that the height of the canopy roughness sublayer, where the effects of surface features are still apparent in the flow, extends between the top of

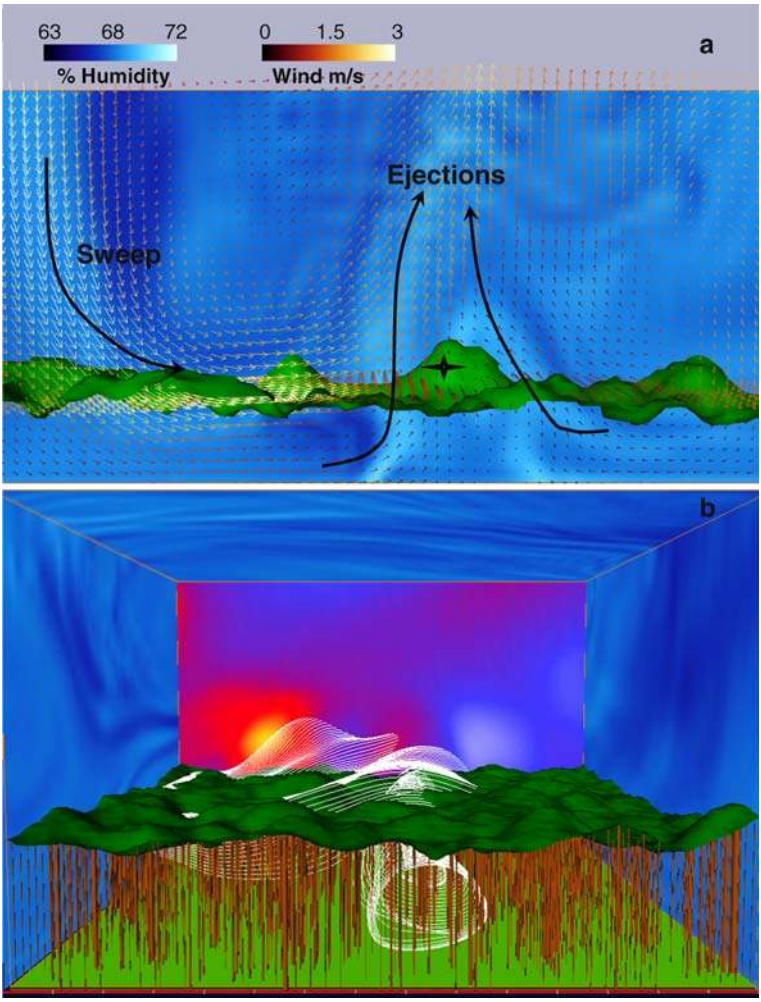

Fig. 7 Snapshots in the HS simulation case: **a** an illustration of the ejection-sweep dynamics and its interaction with canopy structure—the figure illustrates a subsection, 75 m long, 20 m wide and 100 m tall, the canopy top is illustrated as a *green* surface. *Arrows* represent the wind vector, the arrow length and *colour scale* indicating wind speed. The wind vectors are projected on two planes one horizontal at the mean canopy height and the other vertical through the centre of the domain. Water vapour mixing ratio is presented using a blue colour scale and projected on a vertical plain through the back of the domain. A *star* marks a tall cluster of trees at the centre of the domain, and the locations of ejection and sweep events are illustrated with *black arrows*; **b** local circulation inside the canopy sub-domain illustrated with streamlines emanating from a linear source on the left edge of the domain near the canopy top—this figure illustrates a different subsection $150 \times 150 \times 100\,\mathrm{m}^3$. Tree stems are illustrated as *brown lines* (stem diameter in exaggerated scale). Water vapour mixing ratio is projected on the side and top "walls", temperature on the back "wall"

the canopy and up to 2–5 times the canopy height. This definition of the canopy roughness sublayer is analogous to the subdomain in our simulations where the correlation between flux and canopy height is significant. Recent volume-averaged observations from ground-based acoustic Doppler-sodar found that the height of the roughness sublayer was within the same vertical range ($2h_c$–$4h_c$) with a distinct diurnal variation, reaching its maximum under daytime convective conditions (Thomas et al. 2006).

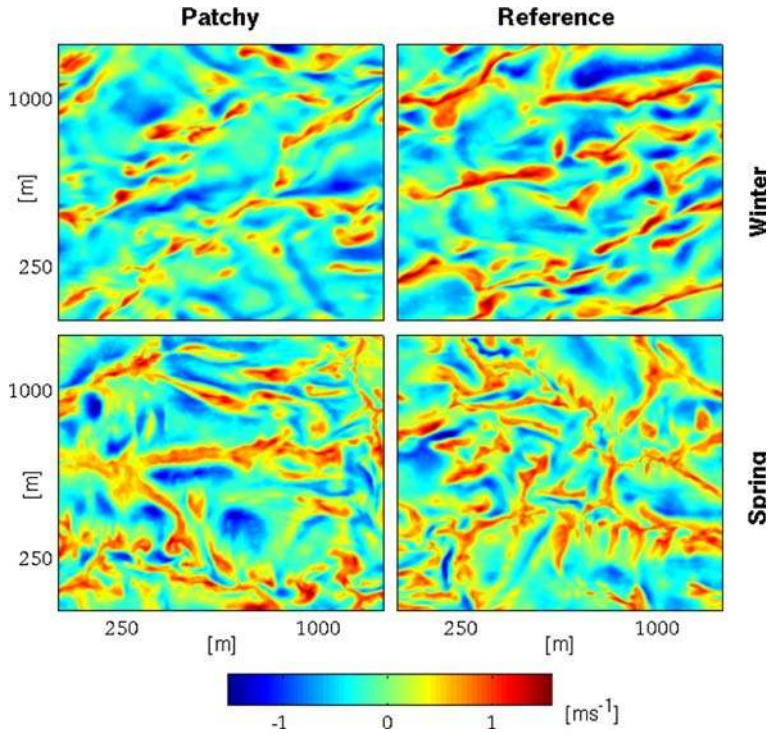

Fig. 8 Snapshots showing the resolved vertical wind component $\overline{w}$ along a horizontal cross section throughout the simulation domain at a height of 40 m above ground level. These snapshots where taken (arbitrarily) at the 15th min of analyzed time of the simulation. They illustrate the eddy structures in each simulation case. Mean integral lengths for each case are indicated in Table 2

5 Conclusions

RAFLES was proposed as a simulation platform to explore how canopy heterogeneity at the scale of tree-fall gaps affects the first and second moments of the flow and scalar fluxes. Overall, the resolution, realistic representation of the canopy, and mesoscale-based initialization and forcing allowed RAFLES to simulate turbulence that compared well with observations. Yet, as was demonstrated in the winter case, which was characterized by a sparse canopy, stronger wind shear above the canopy and weaker surface heat fluxes, an appropriate parameterization of SGS TKE in heterogeneous canopies is still required. Recently proposed dynamic schemes for SGS TKE (e.g., Basu and Porté-Agel 2006; Stoll and Porte-Agel 2006a; Bou-Zeid et al. 2007; Yue et al. 2007, 2008) are based on filtering of the resolved variables across several grid elements and the interpretation of this filtering within a heterogeneous, volume-restricted, canopy sub-domain is not obvious. In addition, these schemes are applied in pseudo-spectral simulations and cannot easily represent explicit sharp boundaries, such as the boundary around a tree-fall gap.

Anthropogenic and natural changes to canopy structure, such as selective logging (Asner et al. 2004), fire (Chambers et al. 2005), regional climate change (Breshears et al. 2005), or bark beetle infestations (Negrón et al. 2000), strongly affect the microscale canopy structure by changing the stand density, leaf density distribution, and distribution of stem sizes. These

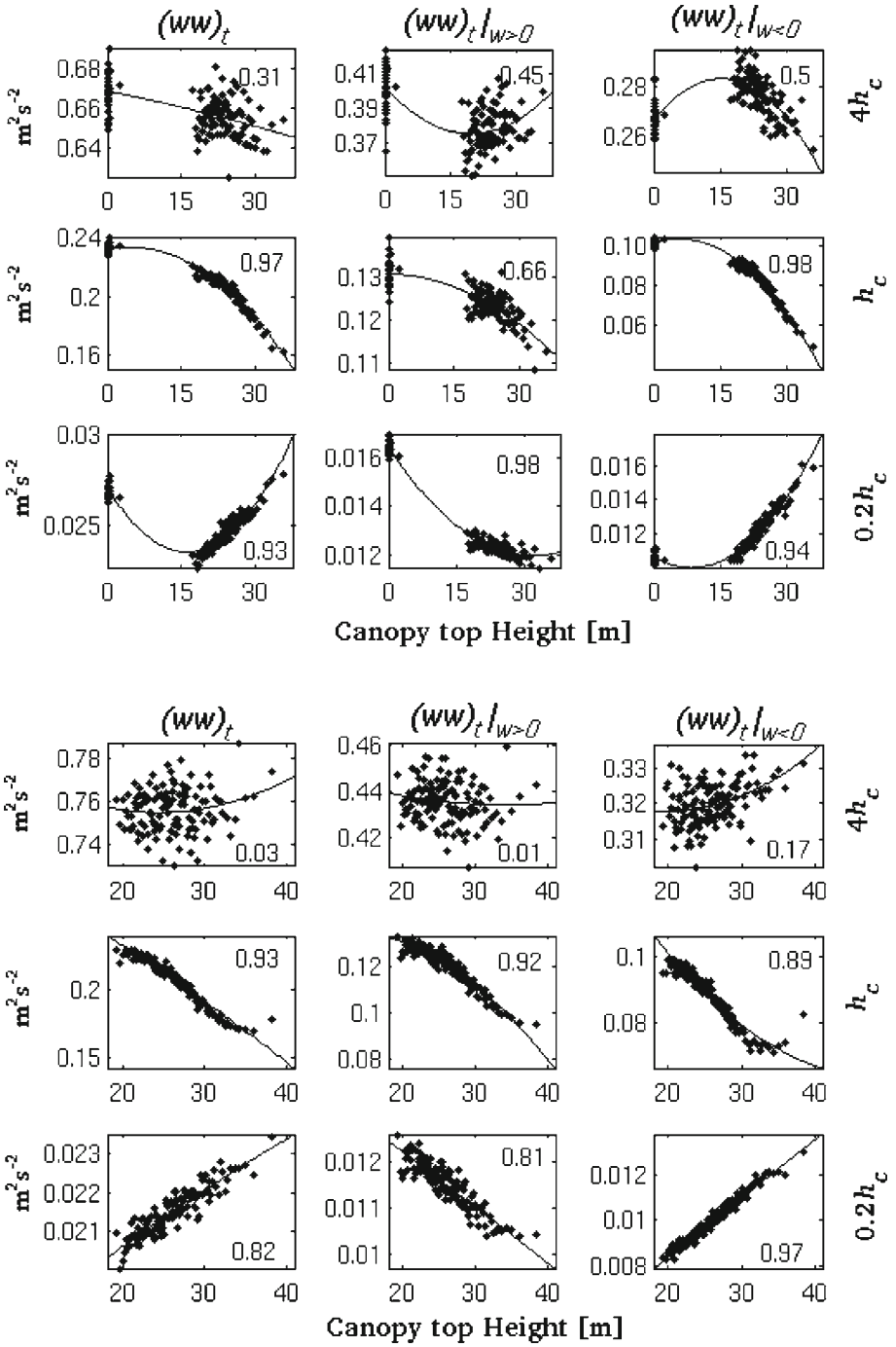

Fig. 9 Correlation between $(ww)_t$ and canopy-top height at three levels for the winter patchy simulation (*top panel*) and winter reference simulation (*bottom panel*). Number at the corners of each figure mark the r^2 for a second-order polynomial line fit (*thin line*)

disturbances create a structural pattern at the length scale of a single tree crown, but such small-scale changes to canopy structure can extend over very large spatial domains (e.g., Asner et al. 2005). Historically, it was assumed that turbulence mixing 'wipes' out such fine scale heterogeneities. As our simulations have shown, eddy mixing length inside, and just above, the canopy sublayer is at the same scale as the tree-crown diameter and, therefore, crown-scale heterogeneity leads to persistent effects, which, under some conditions, are not entirely mixed out even at $4h_c$.

Moving downwind across a heterogeneous canopy, the flow experiences frequent transitions from forest (i.e. high leaf density) to gap (low leaf density, or open space), and from gap to forest. Flesch and Wilson (1999) observed modifications to the mean wind speed and momentum fluxes along a transition from a forested "block" into a deforested gap with short vegetation. These modifications included reduced wind speed shortly downwind from the forest, followed by increased wind speed and TKE farther downwind, up to $6h_c$ (with a peak around $3h_c$–$4h_c$). The patterns of the gap effects were dependent on the gap width. Using LES, Cassiani et al. (2008) showed that the gap effects may extend vertically above up to $2h_c$ and horizontally up to $7h_c$. Dupont and Brunet (2008b) used LES with a heterogeneous patch structure but assumed within-patch horizontal homogeneity, to confirm an analytically derived hypothesis (Belcher et al. 2003) of an increased gust zone, roughly $3h_c$ behind a gap-to-forest transition. They also showed that the location and intensity of this increased gust zone is affected by the vertical profile of LAI in the forest (Dupont and Brunet 2008a). Based on the observed structure of the Duke Forest, the realistic canopies we used here have an autocorrelation length scale of roughly $2h_c$, which is characteristic of natural vegetation and gap sizes. This means that in our simulated domains the transitions from gap to forest, and from forest to gap, are at about the same length or shorter than the length of the predicted for maximal-effect zone, $3h_c$–$10h_c$.

The simulations have shown that interactions between small-scale canopy structures, at a typical length scale of one tree-crown width, and the turbulent flow within and above the canopy volume, affect biosphere-atmosphere exchange at three levels. In terms of canopy representation in larger scale models (level 1), usually conducted via some scaling length connected to the canopy attributes, RAFLES has shown that canopy heterogeneity decreases the displacement height and increases the roughness length and penetration depth. This result holds promise, in that the maximum leaf area, the fractional area of gaps, and the autocorrelation length of the gap patterns may be the logical choices for scaling variables to adjust the parameterized displacement height, roughness length, and penetration depth in regional models. In terms of canonical (planar-averaged) profiles (level 2), the RAFLES simulations suggested that the aerodynamically effective height of the canopy and the spatially-averaged vertical fluxes can normalize the profiles of fluxes, and the first and second statistical moments of the wind velocity. In fact, the planar-averaged mixing lengths derived from RAFLES for these heterogeneous cases (including gaps) are in agreement with canonical mixing lengths often used in one-dimensional higher-order closure models (Wilson and Shaw 1977; Katul and Albertson 1998; Katul and Chang 1999; Poggi et al. 2004a). Finally, we have shown that the signature of such heterogeneity is most pronounced in the spatial distributions of ejection and sweep event locations. This leads to an effect of ejection and sweep "hot spots" that can affect particle (e.g. seed or pollen) dispersion from these locations (Bohrer et al. 2008b), and which, in turn, can affect the long term viability and genetic heterogeneity of plant populations (Bohrer et al. 2005b; Volis et al. 2005). The correlations between canopy height and flux statistics in the ejection or sweep phases persisted above $3h_c$. Observations at this scale need to be at a high enough resolution to represent the heterogeneity and over a domain large enough to include at least one or two full domains of influence of a single structure, such as

a forest-gap-forest pattern. Currently, such observations are very expensive and laborious. The Canopy Horizontal Array Turbulence Study (CHATS) (Patton et al. 2008) represents the most extensive attempt to date to collect observations of flow in real heterogeneous canopies at such length scales. Improvements to measurement instrumentation such as lidar (Eichinger and Cooper 2007) will enable more measurements at these scales.

Our simulations do not provide finality on how such fine-scale heterogeneity affects momentum and heat transport within and above canopies, but they do generate initial hypotheses on how to progress to studying tree-scale effects on mass and momentum transport within forested ecosystems. The simulations of 3-D canopies that include the within-patch crown-scale heterogeneity of canopy structure, as represented in RAFLES, are therefore an essential tool for generating hypotheses and serving as a virtual laboratory to study the effects of small-scale surface heterogeneity.

Acknowledgements We wish to thank Shanti Bhushan for help in implementation of the backscatter scheme, Mario Siquiera and Paul Stoy for providing the eddy-flux observations, Ram Oren, Heather McCarthy, Chris Oishi, Hyun-Seuk Kim, Michael Wolosin, and Mathieu Therezien for canopy structure data, John Albertson, Amilcare Porporato, Matteo Detto and Massimo Cassiani for advice in data analysis, Heidi Holder for comments on an early version, Martin Otte and Ron Stubbs for IT support, and three anonymous reviewers for insightful comments on the manuscript. This study was funded in part by NOAA grant #NA030AR4310150 and NSF grants #IBN-9981620, #DEB-0453665, and #EAR-0628342. The Duke Forest turbulence data were supported by the US Department of Energy (DOE) through the Office of Biological and Environmental Research (BER) Terrestrial Carbon Processes (TCP) program (Grants # 10509-0152, DE-FG02-00ER53015, and DE-FG02-95ER62083). GB was supported in part by the John and Elaine Fellowship through the Harvard University Center for the Environment.

References

Adcroft A, Hill C, Marshall J (1997) Representation of topography by shaved cells in a height coordinate ocean model. Mon Weather Rev 125: 2293–2315

Albertson JD, Katul GG, Wiberg P (2001) Relative importance of local and regional controls on coupled water, carbon, and energy fluxes. Adv Water Resour 24:1103–1118

Arakawa A, Lamb VR (1977) Computational design of the basic dynamical processes of the UCLA general circulation model. In: Chang J (ed) Methods in computational physics: advances in research and applications. Academic Press, London, pp 174–265

Asner GP, Keller M, Silva JNM (2004) Spatial and temporal dynamics of forest canopy gaps following selective logging in the eastern Amazon. Glob Chang Biol 10:765–783

Asner GP, Knapp DE, Broadbent EN, Oliveira PJC, Keller M, Silva JN (2005) Selective logging in the Brazilian Amazon. Science 310:480–482

Avissar R, Schmidt T (1998) An evaluation of the scale at which ground-surface heat flux patchiness affects the convective boundary layer using large-eddy simulations. J Atmos Sci 55:2666–2689

Avissar R, Eloranta EW, Gurer K, Tripoli GJ (1998) An evaluation of the large-eddy simulation option of the regional atmospheric modeling system in simulating a convective boundary layer: a FIFE case study. J Atmos Sci 55:1109–1130

Baldocchi D, Finnigan J, Wilson K, Paw U KT, Falge E (2000) On measuring net ecosystem carbon exchange over tall vegetation on complex terrain. Boundary-Layer Meteorol 96:257–291

Basu S, Porté-Agel F (2006) Large-eddy simulations of stably stratified atmospheric boundary layer turbulence: a scale-dependent dynamic modeling approach. J Atmos Sci 63:2074–2091

Belcher SE, Jerram N, Hunt JCR (2003) Adjustment of a turbulent boundary layer to a canopy of roughness elements. J Fluid Mech 488:369–398

Belcher SE, Finnigan JJ, Harman IN (2008) Flows through forest canopies in complex terrain. Ecol Appl 18:1436–1453

Bhushan S, Warsi ZUA (2005) Large eddy simulation of turbulent channel flow using an algebraic model. Int J Numer Methods Fluids 49:489–519

Bhushan S, Warsi ZUA, Walters DK (2006) Modeling of energy backscatter via an algebraic subgrid-stress model. AIAA J 44:837–847

Bohrer G, Mourad H, Laursen TA, Drewry D, Avissar R, Poggi D, Oren R, Katul GG (2005a) Finite-element tree crown hydrodynamics model (FETCH) using porous media flow within branching elements—a new representation of tree hydrodynamics. Water Resour Res 41:W11404. doi:10.1029/2005WR004181

Bohrer G, Nathan R, Volis S (2005b) Effects of long-distance dispersal for metapopulation survival and genetic structure at ecological time and spatial scales. J Ecol 93:1029–1040

Bohrer G, Wolosin M, Brady R, Avissar R (2007) A virtual canopy generator (V-CaGe) for modeling complex heterogeneous forest canopies at high resolution. Tellus Ser B Chem Phys Meteorol 59:566–576

Bohrer G, Longo M, Zielinski DJ, Brady R (2008a) VR visualisation as an interdisciplinary collaborative data exploration tool for large eddy simulations of biosphere-atmosphere interactions. Advances in visual computing—4th international symposium, ISVC 2008, Las Vegas, NV. Lecture Notes in Computer Science, vol 5358, pp 866–876

Bohrer G, Nathan R, Katul GG, Walko RL, Avissar R (2008b) Effects of canopy heterogeneity, seed abscission, and inertia on wind-driven dispersal kernels of tree seeds. J Ecol 96:569–580

Bou-Zeid E, Meneveau C, Parlange MB (2004) Large-eddy simulation of neutral atmospheric boundary layer flow over heterogeneous surfaces: blending height and effective surface roughness. Water Resour Res 40:WR002475. doi:10.1029/2003WR002475

Bou-Zeid E, Parlange MB, Meneveau C (2007) On the parameterization of surface roughness at regional scales. J Atmos Sci 64:216–227

Bou-Zeid E, Vercauteren N, Parlange MB, Meneveau C (2008) Scale dependence of subgrid-scale model coefficients: an a priori study. Phys Fluid 20:115106

Breshears DD, Cobb NS, Rich PM, Price KP, Allen CD, Balice RG, Romme WH, Kastens JH, Floyd ML, Belnap J, Anderson JJ, Myers OB, Meyer CW (2005) Regional vegetation die-off in response to global-change-type drought. Proc Natl Acad Sci USA 102:15144–15148

Cassiani M, Katul GG, Albertson JD (2008) The effects of canopy leaf area index on airflow across forest edges: large eddy simulation and analytical results. Boundary-Layer Meteorol 126:433–460

Cava D, Katul GG (2008) Spectral short-circuiting and wake production within the canopy trunk space of an alpine hardwood forest. Boundary-Layer Meteorol 126:415–431

Chambers SD, Beringer J, Randerson JT, Chapin FS (2005) Fire effects on net radiation and energy partitioning: contrasting responses of tundra and boreal forest ecosystems. J Geophys Res 110:D09106. doi:10.1029/2004JD005299

Chow FK, Street RL, Xue M, Ferziger JH (2005) Explicit filtering and reconstruction turbulence modeling for large-eddy simulation of neutral boundary layer flow. J Atmos Sci 62:2058–2077

Clark DB, Olivas PC, Oberbauer SF, Clark DA, Ryan MG (2008) First direct landscape-scale measurement of tropical rain forest leaf area index, a key driver of global primary productivity. Ecol Lett 11:163–172

Collins DC, Avissar R (1994) An evaluation with the fourier amplitude sensitivity test (Fast) of which land-surface parameters are of greatest importance in atmospheric modeling. J Clim 7:681–703

Deardorff JW (1980) Stratocumulus-capped mixed layers derived from a 3-dimensional model. Boundary-Layer Meteorol 18:495–527

Detto M, Montaldo N, Albertson JD, Mancini M, Katul G (2006) Soil moisture and vegetation controls on evapotranspiration in a heterogeneous Mediterranean ecosystem on Sardinia, Italy. Water Resour Res 42:W08419. doi:10.1029/2005WR004693

Detto M, Katul GG, Siqueira M, Juang J-H, Stoy PC (2008) The structure of turbulence near a tall forest edge: the backward facing step flow analogy revisited. Ecol Appl 18:1420–1435

Dias MAFS, Regnier P (1996) Simulation of mesoscale circulations in a deforested area of Rondônia in the dry season. In: Gash JHC, Nobre CA, Roberts JM, Victoria RL (eds) Amazonian deforestation and climate. Wiley, Chichester, pp 531–547

Dupont S, Brunet Y (2008a) Influence of foliar density profile on canopy flow: a large-eddy simulation study. Agric Meteorol 148:976–990

Dupont S, Brunet Y (2008b) Edge flow and canopy structure: a large-eddy simulation study. Boundary-Layer Meteorol 126:51–71

Dwyer MJ, Patton EG, Shaw RH (1997) Turbulent kinetic energy budgets from a large-eddy simulation of airflow above and within a forest canopy. Boundary-Layer Meteorol 84:23–43

Eichinger WE, Cooper DI (2007) Using lidar remote sensing for spatially resolved measurements of evaporation and other meteorological parameters. Agron J 99:255–271

Finnigan J (2000) Turbulence in plant canopies. Annu Rev Fluid Mech 32:519–571

Finnigan J (2004) The footprint concept in complex terrain. Agric Meteorol 127:117–129

Fisch G, Culf AD, Nobre CA (1996) Modelling convective boundary layer growth in Rondônia. In: Gash JHC, Nobre CA, Roberts JM, Victoria RL (eds) Amazonian deforestation and climate. Wiley, Chichester, pp 425–435

Flesch TK, Wilson JD (1999) Wind and remnant tree sway in forest cutblocks. I. Measured winds in experimental cutblocks. Agric Meteorol 93:229–242
Foken T, Leclerc MY (2004) Methods and limitations in validation of footprint models. Agric Meteorol 127:223–234
Hadfield MG, Cotton WR, Pielke RA (1991) Large-eddy simulations of thermally forced circulations in the convective boundary-layer. 1. A small-scale circulation with zero wind. Boundary-Layer Meteorol 57: 79–114
Haltiner GJ, Williams RT (1980) Numerical prediction and dynamic meteorology. Wiley, New York, 477 pp
Harman IN, Finnigan JJ (2007) A simple unified theory for flow in the canopy and roughness sublayer. Boundary-Layer Meteorol 123:339–363
Hsieh CI, Katul G, Chi T (2000) An approximate analytical model for footprint estimation of scaler fluxes in thermally stratified atmospheric flows. Adv Water Resour 23:765–772
Hsieh CI, Siqueira M, Katul G, Chu CR (2003) Predicting scalar source-sink and flux distributions within a forest canopy using a 2-D Lagrangian stochastic dispersion model. Boundary-Layer Meteorol 109: 113–138
Hurtt GC, Dubayah R, Drake J, Moorcroft PR, Pacala SW, Blair JB, Fearon MG (2004) Beyond potential vegetation: combining lidar data and a height-structured model for carbon studies. Ecol Appl 14:873–883
Jackson PS (1981) On the displacement height in the logarithmic velocity profile. J Fluid Mech 111:15–25
Juang J-Y, Katul GG, Porporato A, Stoy PC, Siqueira MS, Detto M, Kim HS, Oren R (2007) Eco-hydrological controls on summertime convective rainfall triggers. Glob Chang Biol 13:887–896
Kalnay E, Kanamitsu M, Kistler R, Collins W, Deaven D, Gandin L, Iredell M, Saha S, White G, Woollen J, Zhu Y, Leetmaa A, Reynolds B, Chelliah M, Ebisuzaki W, Higgins W, Janowiak J, Mo KC, Ropelewski C, Wang J, Jenne R, Joseph D (1996) The NCEP/NCAR 40-year reanalysis project. Bull Am Meteorol Soc 77:437–471
Kanda M, Moriwaki R, Kasamatsu F (2004) Large-eddy simulation of turbulent organized structures within and above explicitly resolved cube arrays. Boundary-Layer Meteorol 112:343–368
Katul GG, Albertson JD (1998) An investigation of higher-order closure models for a forested canopy. Boundary-Layer Meteorol 89:47–74
Katul GG, Chang WH (1999) Principal length scales in second-order closure models for canopy turbulence. J Appl Meteorol 38:1631–1643
Katul GG, Chu CR, Parlange MB, Albertson JD, Ortenburger TA (1995) Low-wave-number spectral characteristics of velocity and temperature in the atmospheric surface-layer. J Geophys Res 100:14243–14255
Katul G, Hsieh CI, Kuhn G, Ellsworth DS, Nie DL (1997) Turbulent eddy motion at the forest-atmosphere interface. J Geophys Res 102:13409–13421
Katul GG, Geron CD, Hsieh CI, Vidakovic B, Guenther AB (1998) Active turbulence and scalar transport near the forest-atmosphere interface. J Appl Meteorol 37:1533–1546
Katul G, Hsieh CI, Bowling D, Clark K, Shurpali N, Turnipseed A, Albertson J, Tu K, Hollinger D, Evans B, Offerle B, Anderson D, Ellsworth D, Vogel C, Oren R (1999) Spatial variability of turbulent fluxes in the roughness sublayer of an even-aged pine forest. Boundary-Layer Meteorol 93:1–28
Katul GG, Mahrt L, Poggi D, Sanz C (2004) One- and two-equation models for canopy turbulence. Boundary-Layer Meteorol 113:81–109
Katul GG, Poggi D, Cava D, Finnigan J (2006) The relative importance of ejections and sweeps to momentum transfer in the atmospheric boundary layer. Boundary-Layer Meteorol 120:367–375
Klemp JB, Wilhelmson RB (1978) Simulation of 3-dimensional convective storm dynamics. J Atmos Sci 35:1070–1096
Kruijt B, Elbers JA, von Randow C, Araujo AC, Oliveira PJ, Culf A, Manzi AO, Nobre AD, Kabat P, Moors EJ (2004) The robustness of eddy correlation fluxes for Amazon rain forest conditions. Ecol Appl 14:S101–S113
Launiainen S, Vesala T, Mölder M, Mammarella I, Smolander S, Rannik Ü, Kolar P, Har P, Lindroth A, Katul GG (2007) Vertical variability and effect of stability on turbulence characteristics down to the floor of a pine forest. Tellus Ser B Chem Phys Meteorol 59:919–936
Lefsky MA, Cohen WB, Parker GG, Harding DJ (2002) Lidar remote sensing for ecosystem studies. Bioscience 52:19–30
Li B, Avissar R (1994) The impact of spatial variability of land-surface characteristics on land-surface heat fluxes. J Clim 7:527–537
Liu YQ, Avissar R (1996) Sensitivity of shallow convective precipitation induced by land surface heterogeneities to dynamical and cloud microphysical parameters. J Geophys Res 101:7477–7497
Massman WJ, Weil JC (1999) An analytical one-dimensional second-order closure model of turbulence statistics and the Lagrangian time scale within and above plant canopies of arbitrary structure. Boundary-Layer Meteorol 91:81–107

McCarthy HR, Oren R, Finzi AC, Ellsworth DS, Kim H-S, Johnsen KH, Millar B (2007) Temporal dynamics and spatial variability in the enhancement of canopy leaf area under elevated atmospheric CO_2. Glob Chang Biol 13:2479–2497

Medvigy D, Walko RL, Avissar R (2008) Modeling interannual variability of the Amazon hydroclimate. Geophys Res Lett 35. doi:10.1029/2008GL034941

Meyers TP, Baldocchi DD (1991) The budgets of turbulent kinetic-energy and Reynolds stress within and above a deciduous forest. Agric Meteorol 53:207–222

Moorcroft PR, Hurtt GC, Pacala SW (2001) A method for scaling vegetation dynamics: the ecosystem demography model (ED). Ecol Monogr 71:557–585

Naidu SL, DeLucia EH, Thomas RB (1998) Contrasting patterns of biomass allocation in dominant and suppressed loblolly pine. Can J Res 28:1116–1124

Nakai T, Sumida A, Matsumoto K, Daikoku K, Iida S, Park H, Miyahara M, Kodama Y, Kononov AV, Maximov TC, Yabuki H, Hara T, Ohta T (2008) Aerodynamic scaling for estimating the mean height of dense canopies. Boundary-Layer Meteorol 128:423–443

Negrón JF, Wilson JL, Anhold JA (2000) Stand conditions associated with roundheaded pine beetle (Coleoptera: Scolytidae) infestations in Arizona and Utah. Environ Entomol 29:20–27

Nepf H, Ghisalberti M, White B, Murphy E (2007) Retention time and dispersion associated with submerged aquatic canopies. Water Resour Res 43:W04422. doi:10.1029/2006WR005362

Novick KA, Stoy PC, Katul GG, Ellsworth DS, Siqueira MBS, Juang J, Oren R (2004) Carbon dioxide and water vapor exchange in a warm temperate grassland. Oecologia 138:259–274

Oren R, Hseih CI, Stoy P, Albertson J, McCarthy HR, Harrell P, Katul GG (2006) Estimating the uncertainty in annual net ecosystem carbon exchange: spatial variation in turbulent fluxes and sampling errors in eddy-covariance measurements. Glob Chang Biol 12:883–896

Orlanski I (1975) A rational subdivision of scales for atmospheric processes. Bull Am Meteorol Soc 56:527–530

Palace M, Keller M, Asner GP, Hagen S, Braswell B (2008) Amazon forest structure from IKONOS satellite data and the automated characterization of forest canopy properties. Biotropica 40:141–150

Patton EG (1997) Large-eddy simulation of turbulent flow above and within a plant canopy. Atmospheric Science, University of California Davis, 132 pp

Patton EG, Horst TW, Lenschow DH, Sullivan PP, Oncley S, Burns S, Guenther A, Held A, Karl T, Mayor S, Rizzo L, Spuler S, Sun J, Turnipseed A, Allwine E, Edburg S, Lamb B, Avissar R, Holder HE, Calhoun R, Kleissl J, Massman W, Paw U KT, Weil JC (2008) The canopy horizontal array turbulecne study (CHATS). In: The 18th symposium on boundary layers and turbulence

Pielke RA, Cotton WR, Walko RL, Tremback CJ, Lyons WA, Grasso LD, Nicholls ME, Moran MD, Wesley DA, Lee TJ, Copeland JH (1992) A comprehensive meteorological modeling system—RAMS. Meteorol Atmos Phys 49:69–91

Poggi D, Katul GG (2006) Two-dimensional scalar spectra in the deeper layers of a dense and uniform model canopy. Boundary-Layer Meteorol 121:267–281

Poggi D, Katul GG, Albertson JD (2004a) Momentum transfer and turbulent kinetic energy budgets within a dense model canopy. Boundary-Layer Meteorol 111:589–614

Poggi D, Porporato A, Ridolfi L, Albertson JD, Katul GG (2004b) Interaction between large and small scales in the canopy sublayer. Geophys Res Lett 31:L05102. doi:10.1029/2003GL018611

Poggi D, Porporato A, Ridolfi L, Albertson JD, Katul GG (2004c) The effect of vegetation density on canopy sub-layer turbulence. Boundary-Layer Meteorol 111:565–587

Prabha TV, Karipot A, Binford MW (2007) Characteristics of secondary circulations over an inhomogeneous surface simulated with large-eddy simulation. Boundary-Layer Meteorol 123:239–261

Rannik Ü, Aubinet M, Kurbanmuradov O, Sabelfeld KK, Markkanen T, Vesala T (2000) Footprint analysis for measurements over a heterogeneous forest. Boundary-Layer Meteorol 97:137–166

Raupach MR (1989a) Applying Lagrangian fluid-mechanics to infer scalar source distributions from concentration profiles in plant canopies. Agric Meteorol 47:85–108

Raupach MR (1989b) A practical Lagrangian method for relating scalar concentrations to source distributions in vegetation canopies. Q J Roy Meteorol Soc 115:609–632

Raupach MR, Thom AS (1981) Turbulence in and above plant canopies. Annu Rev Fluid Mech 13:97–129

Raupach MR, Finnigan JJ, Brunet Y (1996) Coherent eddies and turbulence in vegetation canopies: the mixing-layer analogy. Boundary-Layer Meteorol 78:351–382

Scanlon TM, Albertson JD (2003) Water availability and the spatial complexity of CO_2, water, and energy fluxes over a heterogeneous sparse canopy. J Hydrometeorol 4:798–809

Schäfer KVR (2002) Effects of increased atmospheric CO_2 concentrations on water and carbon relations of four co-occurring tree species. Nicolas School of the Environment and Earth Sciences, Duke University, 208 pp

Schmid HP (2002) Footprint modeling for vegetation atmosphere exchange studies: a review and perspective. Agric Meteorol 113:159–183
Shaw RH, Patton EG (2003) Canopy element influences on resolved- and subgrid-scale energy within a large-eddy simulation. Agric Meteorol 115:5–17
Shaw RH, Schumann U (1992) Large-eddy simulation of turbulent-flow above and within a forest. Boundary-Layer Meteorol 61:47–64
Shaw RH, Denhartog G, Neumann HH (1988) Influence of foliar density and thermal-stability on profiles of reynolds stress and turbulence intensity in a deciduous forest. Boundary-Layer Meteorol 45:391–409
Sogachev A, Leclerc MY, Karipot A, Zhang G, Vesala T (2005) Effect of clearcuts on footprints and flux measurements above a forest canopy. Agric Meteorol 133:182–196
Stoll R, Porte-Agel F (2006a) Dynamic subgrid-scale models for momentum and scalar fluxes in large-eddy simulations of neutrally stratified atmospheric boundary layers over heterogeneous terrain. Water Resour Res 42:W01409. doi:10.1029/2005WR003989
Stoll R, Porte-Agel F (2006b) Effect of roughness on surface boundary conditions for large-eddy simulation. Boundary-Layer Meteorol 118:169–187
Stoll R, Porte-Agel F (2008) Large-eddy simulation of the stable atmospheric boundary layer using dynamic models with different averaging schemes. Boundary-Layer Meteorol 126:1–28
Stoy PC, Katul GG, Siqueira MBS, Juang JY, Novick KA, Uebelherr JM, Oren R (2006) An evaluation of models for partitioning eddy covariance-measured net ecosystem exchange into photosynthesis and respiration. Agric Meteorol 141:2–18
Su HB, Shaw RH, Paw U KT, Moeng CH, Sullivan PP (1998) Turbulent statistics of neutrally stratified flow within and above a sparse forest from large-eddy simulation and field observations. Boundary-Layer Meteorol 88:363–397
Su HB, Schmid HP, Vogel CS, Curtis PS (2008) Effects of canopy morphology and thermal stability on mean flow and turbulence statistics observed inside a mixed hardwood forest. Agric Meteorol 148:862–882
Thomas C, Foken T (2007) Flux contribution of coherent structures and its implications for the exchange of energy and matter in a tall spruce canopy. Boundary-Layer Meteorol 123:317–337
Thomas C, Mayer JC, Meixner FX, Foken T (2006) Analysis of low-frequency turbulence above tall vegetation using a Doppler sodar. Boundary-Layer Meteorol 119:563–587
Tremback CJ, Walko RL, Bell MJ (2004) RAMS/HYPACT evaluation and visualization utilities, version 2.5 user guide. ATMET LLC, Boulder, CO, 32 pp
Volis S, Bohrer G, Oostermeijer G, Van Tienderen P (2005) Regional consequences of local population demography and genetics in relation to habitat management in *Gentiana pneumonanthe*. Conserv Biol 19: 357–367
Walko RL, Avissar R (2008) The ocean-land-atmosphere model (OLAM). Part II: formulation and tests of the nonhydrostatic dynamic core. Mon Weather Rev 136:4045–4062
Weishampel JF, Drake JB, Cooper A, Blair JB, Hofton M (2007) Forest canopy recovery from the 1938 hurricane and subsequent salvage damage measured with airborne LiDAR. Remote Sens Environ 109:142–153
Wilson NR, Shaw RH (1977) Higher-order closure model for canopy flow. J Appl Meteorol 16:1197–1205
Yang B, Morse AP, Shaw RH, U KTP (2006a) Large-eddy simulation of turbulent flow across a forest edge. Part II: momentum and turbulent kinetic energy budgets. Boundary-Layer Meteorol 121:433–457
Yang B, Raupach M, Shaw RH, U KTP, Morse AP (2006b) Large-eddy simulation of turbulent flow across a forest edge. Part I: flow statistics. Boundary-Layer Meteorol 119:377–412. doi:10.1007/s10546-006-9083-3
Yue W, Parlange MB, Meneveau C, Zhu W, van Hout R, Katz J (2007) Large-eddy simulations of plant canopy flows using plant-scale representation. Boundary-Layer Meteorol 124:183–203. doi:10.1007/s10546-007-9173-x
Yue W, Meneveau C, Parlange MB, Zhu W, Kang HS, Katz J (2008) Turbulent kinetic energy budgets in a model canopy: comparisons between LES and wind-tunnel experiments. Environ Fluid Mech 8:73–95